EUV and Soft X-Ray Beamlines

David Attwood
University of California, Berkeley

Cheiron School
September 2013
SPring-8

Beamlines are used to transport photons to the sample, and take a desired spectral slice

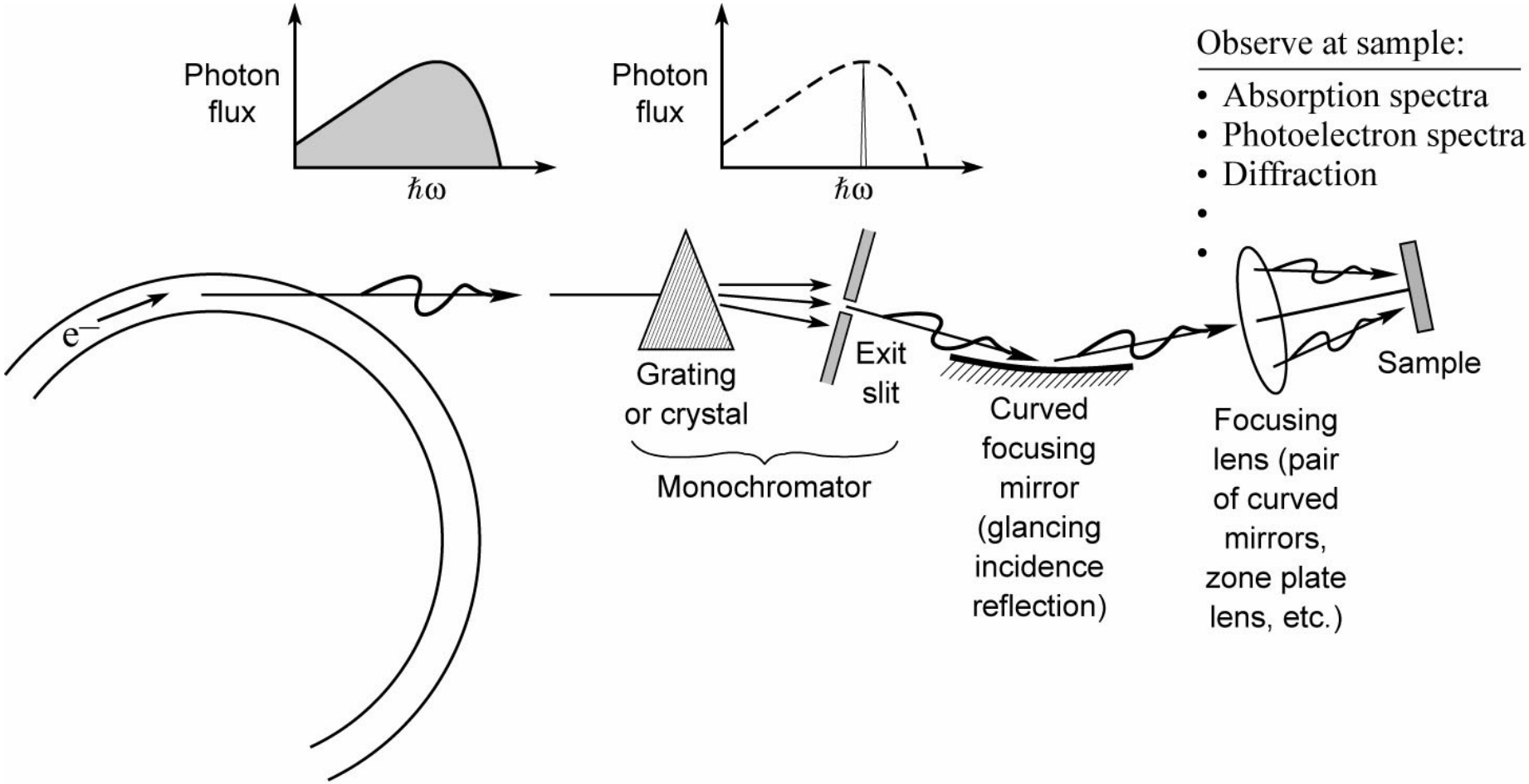

Ch05_F01b_BLtransport.ai

A typical beamline: monochromator plus focusing optics to deliver radiation to the sample

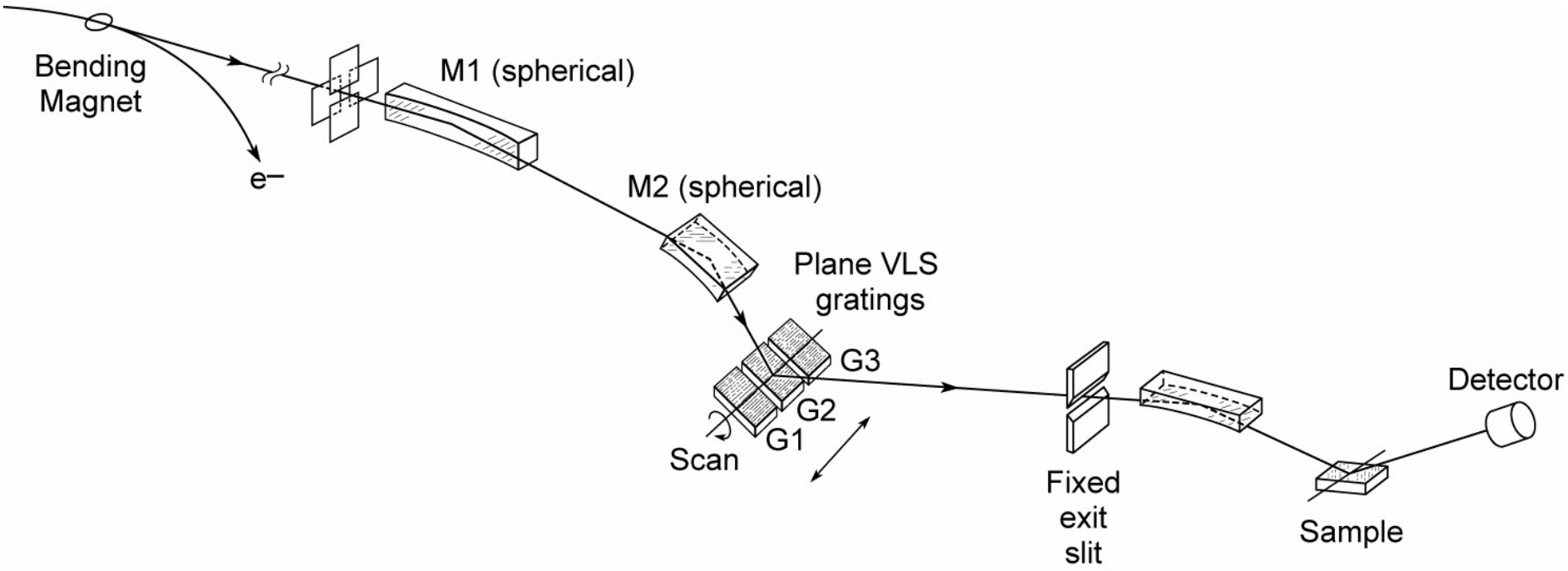

Courtesy of James Underwood (EUV Technology Inc.)

XBD9509-04496_Jan04.ai

Beamline 7.0 at Berkeley's Advanced Light Source

Undulator radiated power in the central cone

$$\lambda_x = \frac{\lambda_u}{2\gamma^2}\left(1 + \frac{K^2}{2} + \gamma^2\theta^2\right)$$

$$\bar{P}_{cen} = \frac{\pi e \gamma^2 I}{\epsilon_0 \lambda_u} \frac{K^2}{\left(1 + \frac{K^2}{2}\right)^2} f(K)$$

$$\theta_{cen} = \frac{1}{\gamma^*\sqrt{N}}$$

$$\left(\frac{\Delta\lambda}{\lambda}\right)_{cen} = \frac{1}{N}$$

$$K = \frac{eB_0\lambda_u}{2\pi m_0 c}$$

$$\gamma^* = \gamma / \sqrt{1 + \frac{K^2}{2}}$$

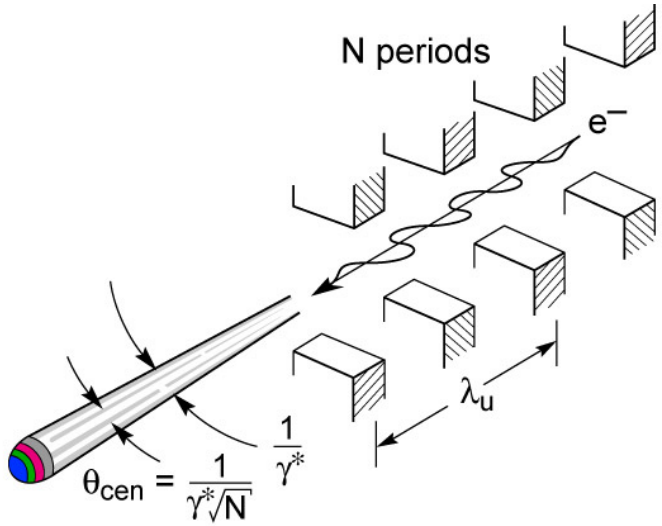

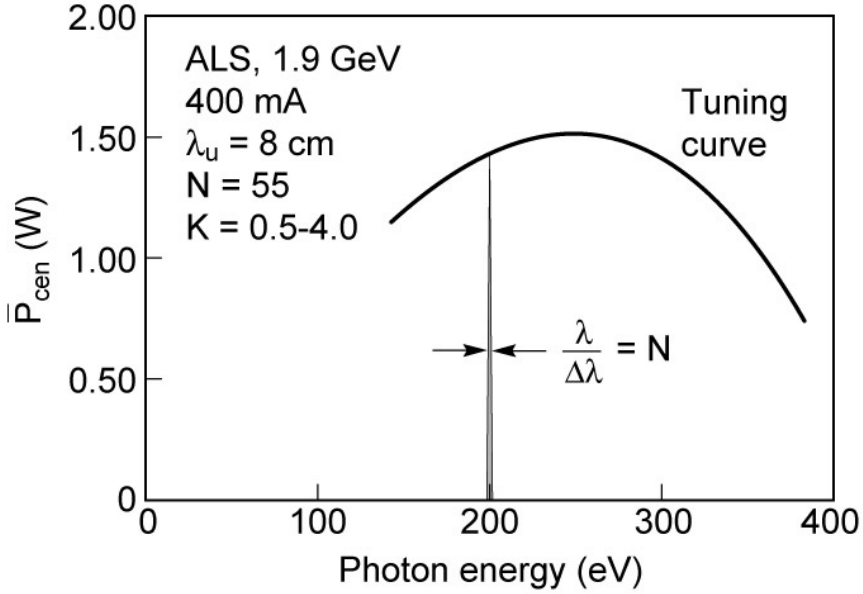

Power in the central radiation cone for three x-ray undulators

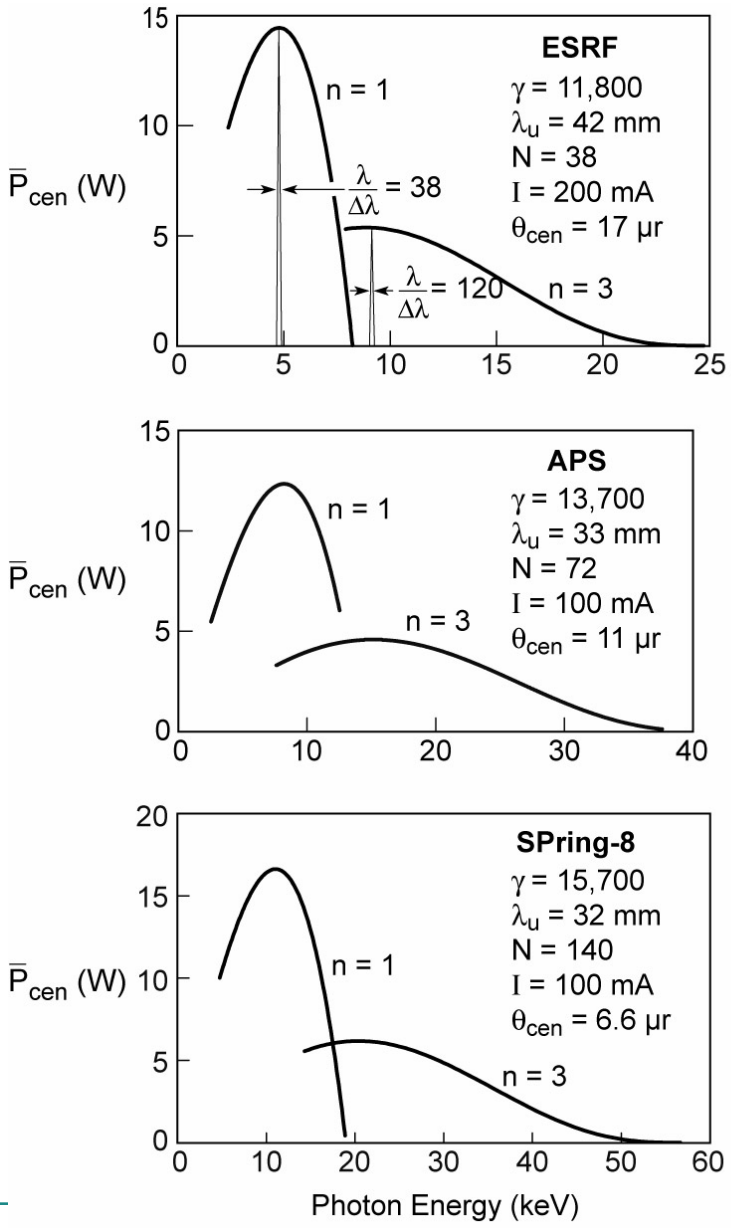

$$\theta_{cen} = \frac{1}{\gamma\sqrt{N}}$$

$$\left[\frac{\Delta\lambda}{\lambda}\right]_1 = \frac{1}{N}$$

$$\left[\frac{\Delta\lambda}{\lambda}\right]_3 = \frac{1}{3N}$$

High spectral resolution (meV beamline)

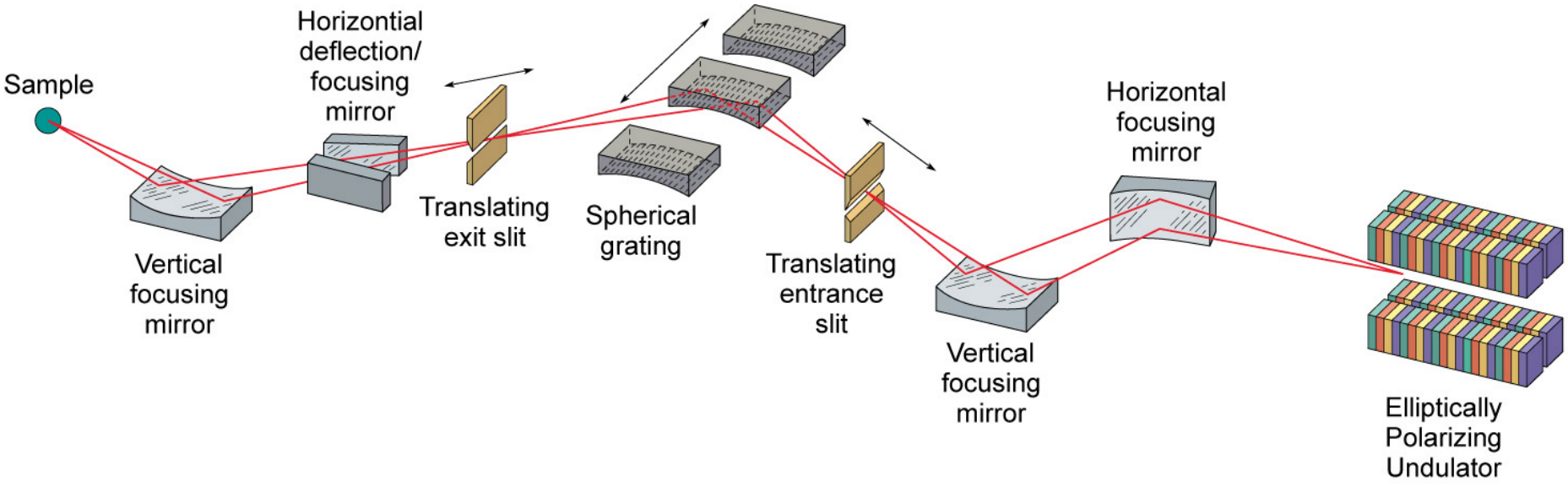

Courtesy of Zahid Hussein (ALS)

MAESTRO: A new varied-line-space grating monochromator beam line for angle-resolved-photo-electron-spectroscopy with high spectral and spatial resolution at the Advanced Light Source

Jason Wells, Derek Yegian, Ken Chow, Eli Rotenberg, Aaron Bostwick, Geoff Gaines and Tony Warwick

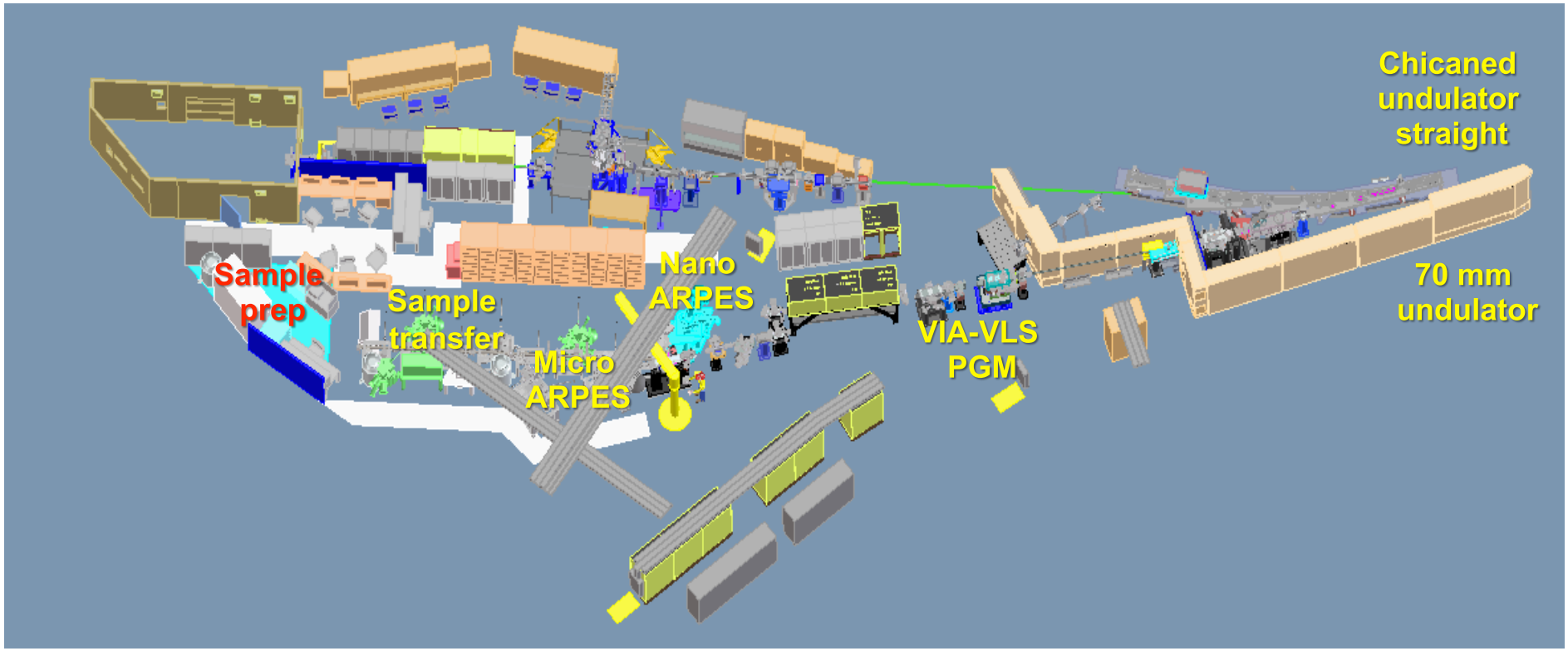

The latest soft x-ray undulator spectroscopy beam line planned for the ALS serves **MAESTRO** a new high resolution Angle Resolved Photo Emission facility with zone-plate focused nano-ARPES. The beam line design offers spectral resolution 1:30000 from 60eV to 400eV with an extended energy range from 20eV to 1000eV. Challenges include optical figure quality, thermal engineering, source size and stability and vibrations in the monochromator. The optical design is radical in that a VLS grating will provide all of the focusing in the dispersion direction, and the mirrors are plane, except for a sphere to collect and focus horizontally.

Courtesy of Eli Rotenberg and Tony Warwick (ALS)

Varied line space gratings

Varied-Line-Space Plane Gratings provide focusing and aberration correction along with the dispersion that they generate in the monochromator. They can be used to erect the monochromator focal plane, making the position of the focus at the exit slit (almost) stationary as the grating rotates to select the photon energy. Beyond that, they are now being used to replace the focusing from shaped optics, making beam lines cheaper and easier to align.

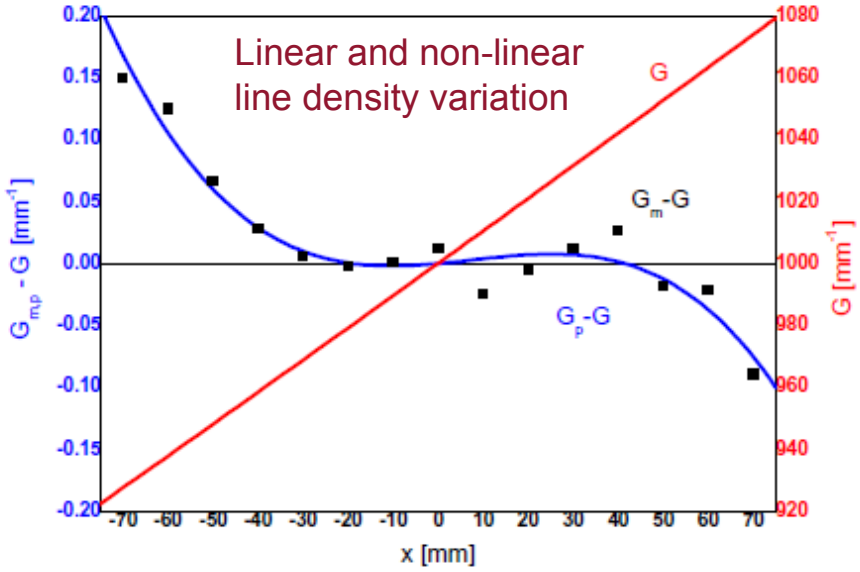

The PEEM3 beam line at 11.0.2 uses a Triple-Ruled Varied-Line-Space grating:

1) to erect the focal plane on a stationary set of exit slits
2) to keep the zero-order light in focus, for easy tuning, and for monitoring of the photon energy.

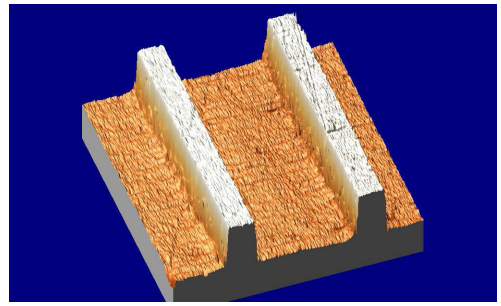

AFM measured groove shapes

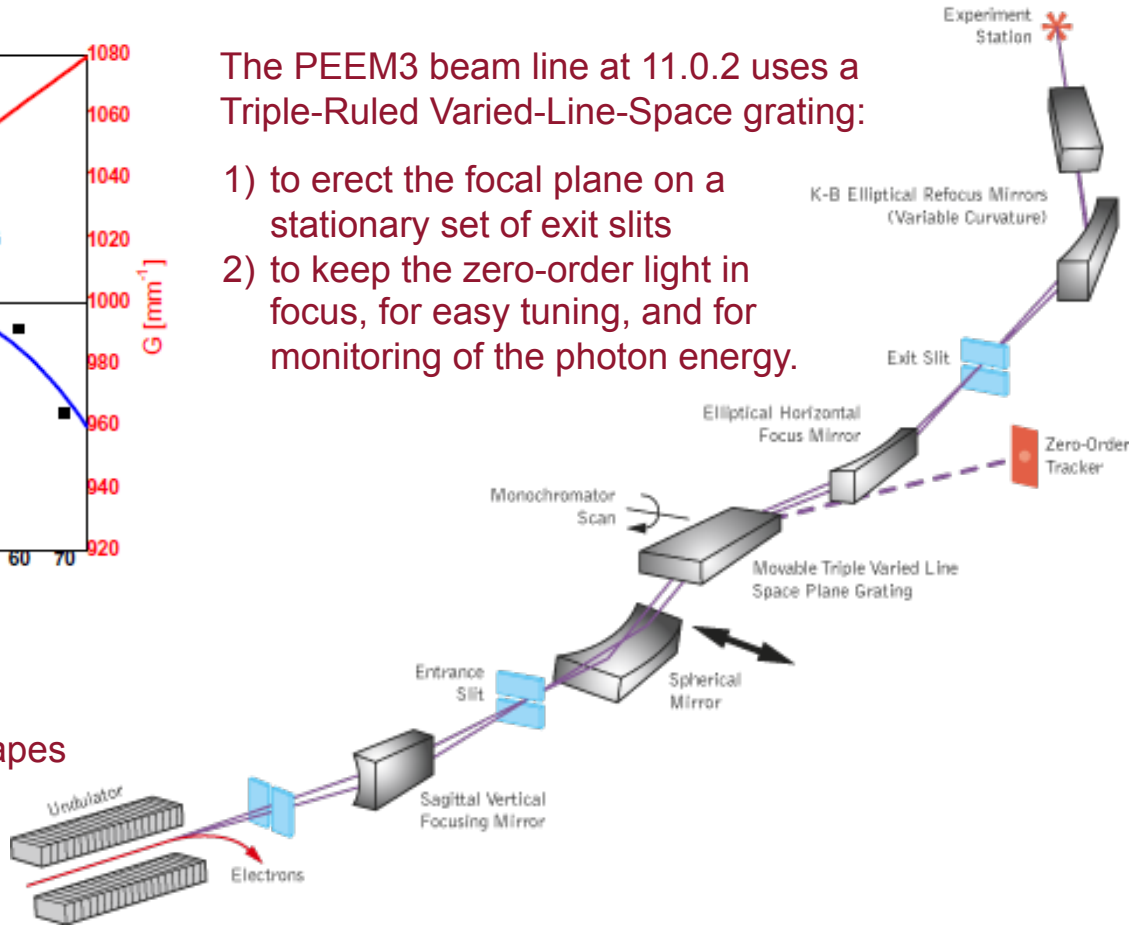

Courtesy of Tony Warwick (ALS)

MAESTRO: A new varied-line-space grating monochromator beam line at the ALS

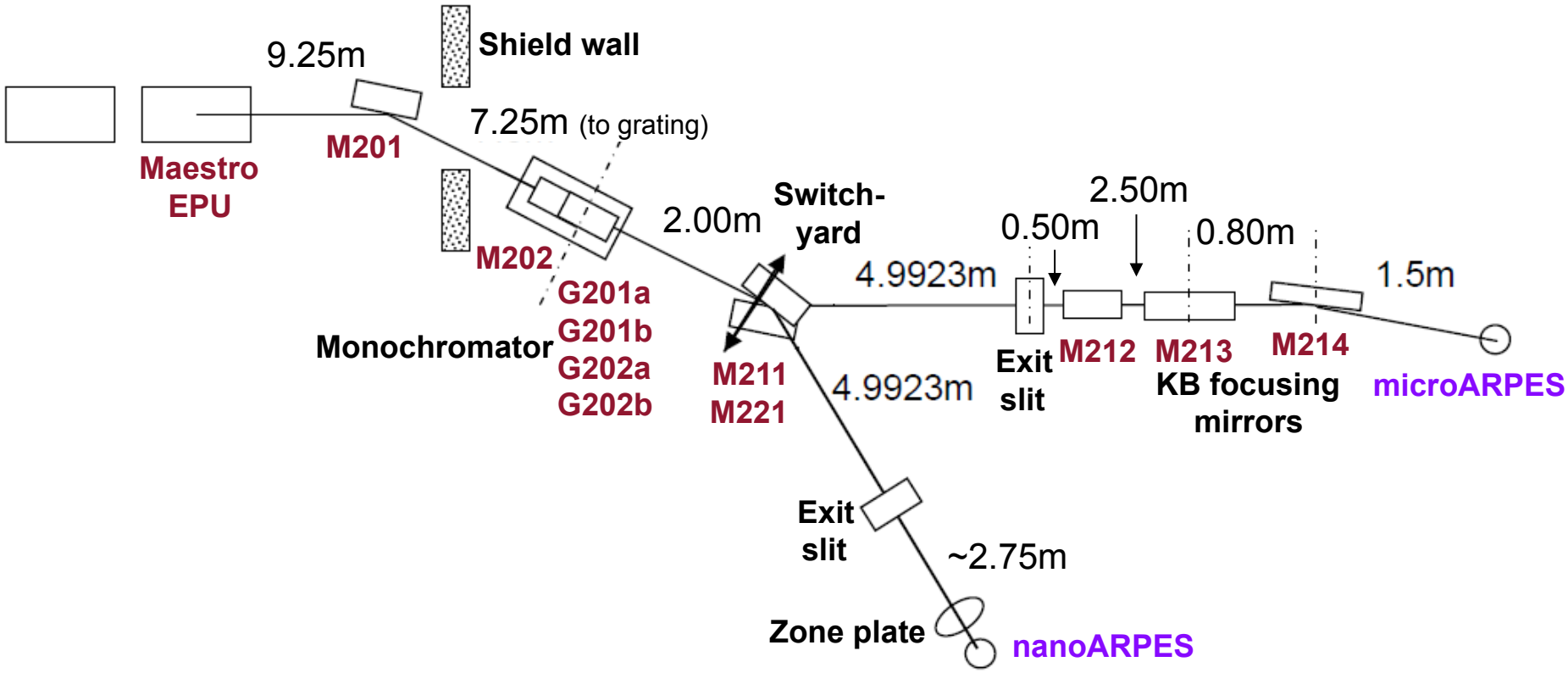

MAESTRO at the ALS: gratings and efficiencies

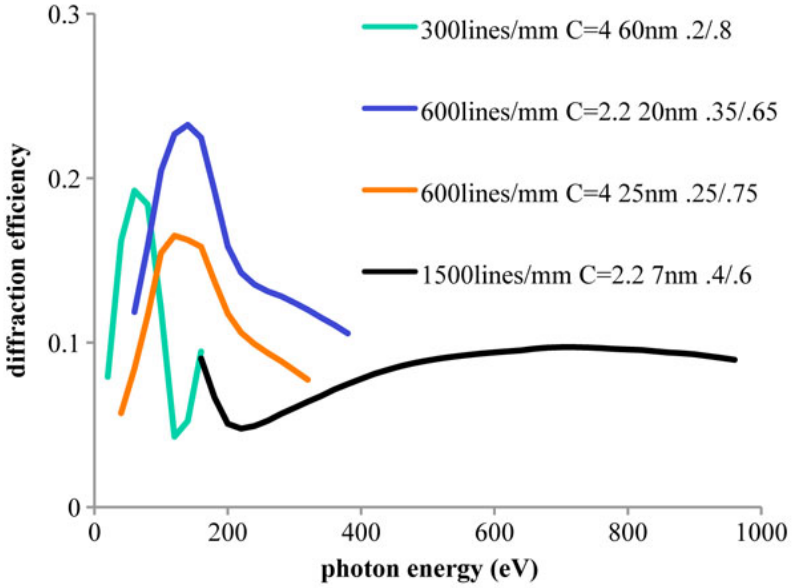

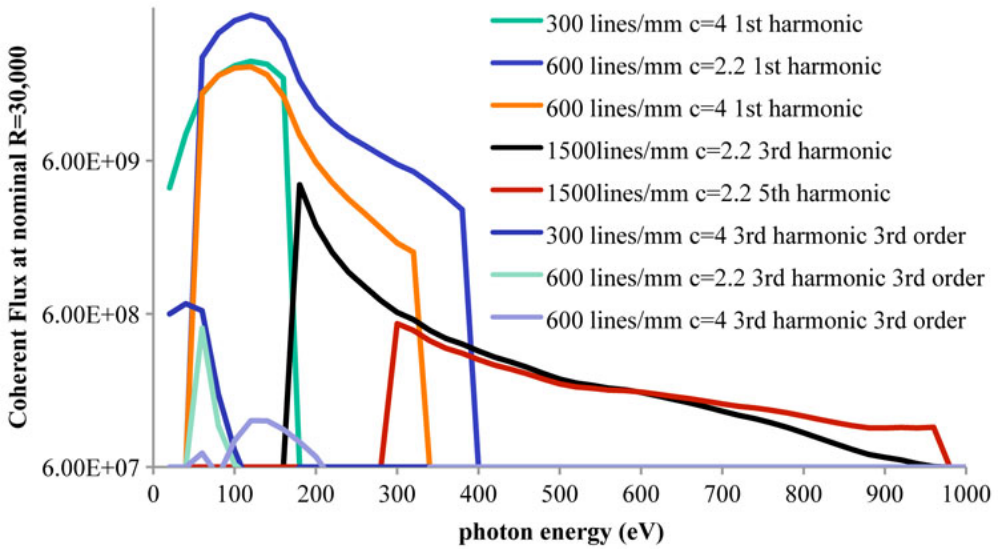

Courtesy of Tony Warwick (ALS)

Water-cooled optics are essential: correcting slope errors due to a thermal bump

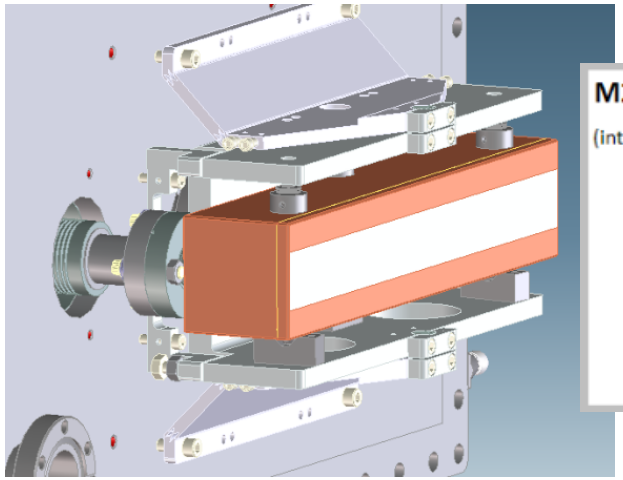

M201 Plane - Slope Errors (µRad) (internally cooled Glidcop, 10K W/m²K)	over full mirror substrate		over clear aperture	
	60eV	20eV	60eV	20eV
Maximum Tangential Slope Error	28.2	61.3	28.2	61.3
Average Tangential Slope Error	2.4	4.9	3.0	6.1
RMS Tangential Slope Error	3.3	7.0	4.4	9.3
Maximum Sagittal Slope Error	36.4	75.1	36.4	75.1
Average Sagittal Slope Error	7.3	15.3	13.9	29.2
RMS Sagittal Slope Error	12.2	25.6	18.0	38.0

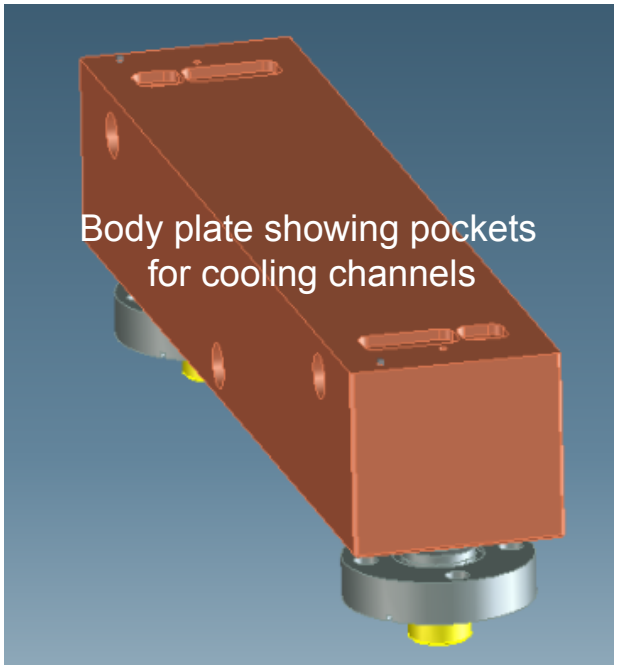

Height error

Tangential slope error

Sagittal slope error

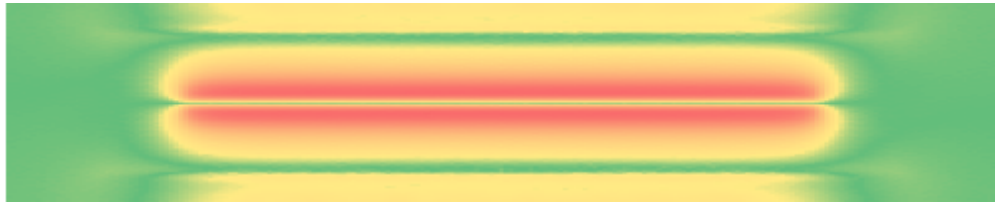

Courtesy of Tony Warwick (ALS)

Ray tracing beamlines is an important tool

Significant degradation of the spectral resolution occurs due to localized heating of M202. It is almost entirely corrected by adjusting the monochromator focusing parameter from 3.93 to 4.02. The engineering design will allow this mirror to be built with 1mm thick hot-wall and the actual thermal deformation is expected to be less.

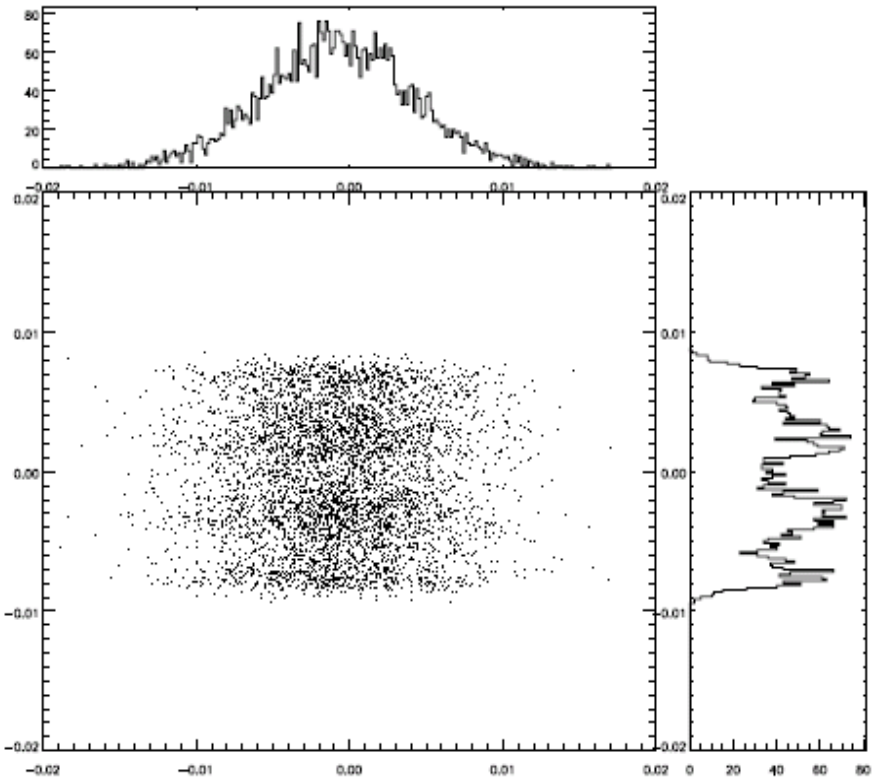

600lines_60eV_10000_c=3.93034_18.7_0.038_
1.5mmheatbump

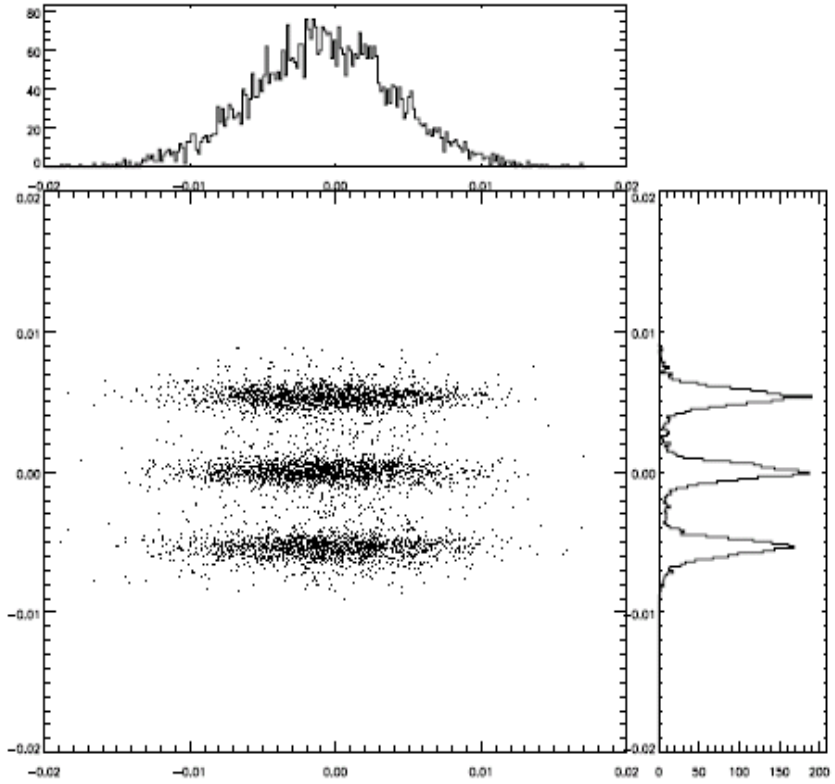

600lines_60eV_10000_c=4.02_18.7_0.038_
1.5mmheatbumpcorrected

Courtesy of Tony Warwick (ALS)

References

Reininger, R., Kriesel, K., Hulbert, S.L., Sanchez-Hanke, C. and Arena, D.A., Rev. Sci. Instrum.,79, 033108 2008

Peterson, H., Jung, C., Hellwig, C. Peatman, W.B. and Gudat, W., Rev. Sci. Instrum. 66 (1995) 1

Follath, R., and Senf, F., Nucl.Intrum. Methods Phys. Res. A390 (1997) 388

Amemiya, K., Kitajima, Y.,Ohta, T., and Ito, K., J. Synchrotron Radiation 3 (1996) 282

The original SHADOW package is available at www.nanotech.wisc.edu/CNTLABS/shadow.html and with an IDL user interface at www.esrf.fr/computing/scientific/xop

Undulator Radiation, Ellaume, P., in Undulators, Wigglers and their Applications,

Onuki, H. and Ellaume, P. eds., Taylor and Francis.

Characteristics of Synchrotron Radiation, Kim, K., J., in Xray Data Booklet LBNL internal report (1986) PUB 490 xdb.lbl.gov/xdb.pdf

D Fluckiger - Grating Solver Development Company Dec 2006 www.gsolver.com

Typical parameters for synchrotron radiation

Facility	ALS	New Subaru	APS	SP-8
Electron energy	1.90 GeV	1.00 GeV	7.00 GeV	8.00 GeV
γ	3720	1957	13,700	15,700
Current (mA)	400	100	100	100
Circumference (m)	197	119	1100	1440
RF frequency (MHz)	500	500	352	509
Pulse duration (FWHM) (ps)	35-70	26	100	120
Bending Magnet Radiation:				
Bending magnet field (T)	1.27	1.03	0.599	0.679
Critical photon energy (keV)	3.05	0.685	19.5	28.9
Critical photon wavelength	0.407 nm	1.81 nm	0.636 Å	0.429 Å
Bending magnet sources	24	4	35	23
Undulator Radiation:				
Number of straight sections	12	4	40	48
Undulator period (typical) (cm)	5.00	5.40	3.30	3.20
Number of periods	89	200	72	140
Photon energy ($K = 1$, $n = 1$)	457 eV	117 eV	9.40 keV	12.7 keV
Photon wavelength ($K = 1$, $n = 1$)	2.71 nm	10.6 nm	1.32 Å	0.979 Å
Tuning range ($n = 1$)	230-620 eV	43-170 eV	3.5-12 keV	4.7-19 keV
Tuning range ($n = 3$)	690-1800 eV	130-500 eV	10-38 keV	16-51 keV
Central cone half-angle ($K = 1$)	35 µrad	44 µrad	11 µrad	6.6 µrad
Power in central cone ($K = 1$, $n = 1$) (W)	2.3	0.15	12	16
Flux in central cone (photons/s)	3.1×10^{16}	7.9×10^{15}	7.9×10^{15}	7.9×10^{15}
σ_x, σ_y (µm)	260, 16	450, 220	320, 50	380, 6.8
σ'_x, σ'_y (µrad)	23, 3.9	89, 18	23, 7	16, 1.8
Brightness ($K = 1$, $n = 1$)[a] [(photons/s)/mm^2 · mrad^2 · (0.1%BW)]	2.3×10^{19}	1.7×10^{17}	5.9×10^{18}	1.8×10^{20}
Total power ($K = 1$, all n, all θ) (W)	83	27	350	2,000
Other undulator periods (cm)	3.65, 8.00, 10.0	7.60	2.70, 5.50, 12.8	2.4, 10.0, 3.7, 12.0
Wiggler Radiation:				
Wiggler period (typical) (cm)	16.0		8.5	12.0
Number of periods	19		28	37
Magnetic field (maximum) (T)	2.1		1.0	1.0
K (maximum)	32		7.9	11
Critical photon energy (keV)	5.1		33	43
Critical photon wavelength	0.24 nm		0.38 Å	0.29 Å
Total power (max. K) (kW)	13		7.4	18

[a]Using Eq. (5.65). See comments following Eq. (5.64) for the case where $\sigma'_{x,y} \simeq \theta_{cen}$.

Time structure of synchrotron radiation

The axial electric field within the RF cavity, used to replenish lost (radiated) energy, forms a potential well "bucket" system that forces electrons into axial electron "bunches". This leads to a time structure in the emitted radiation.

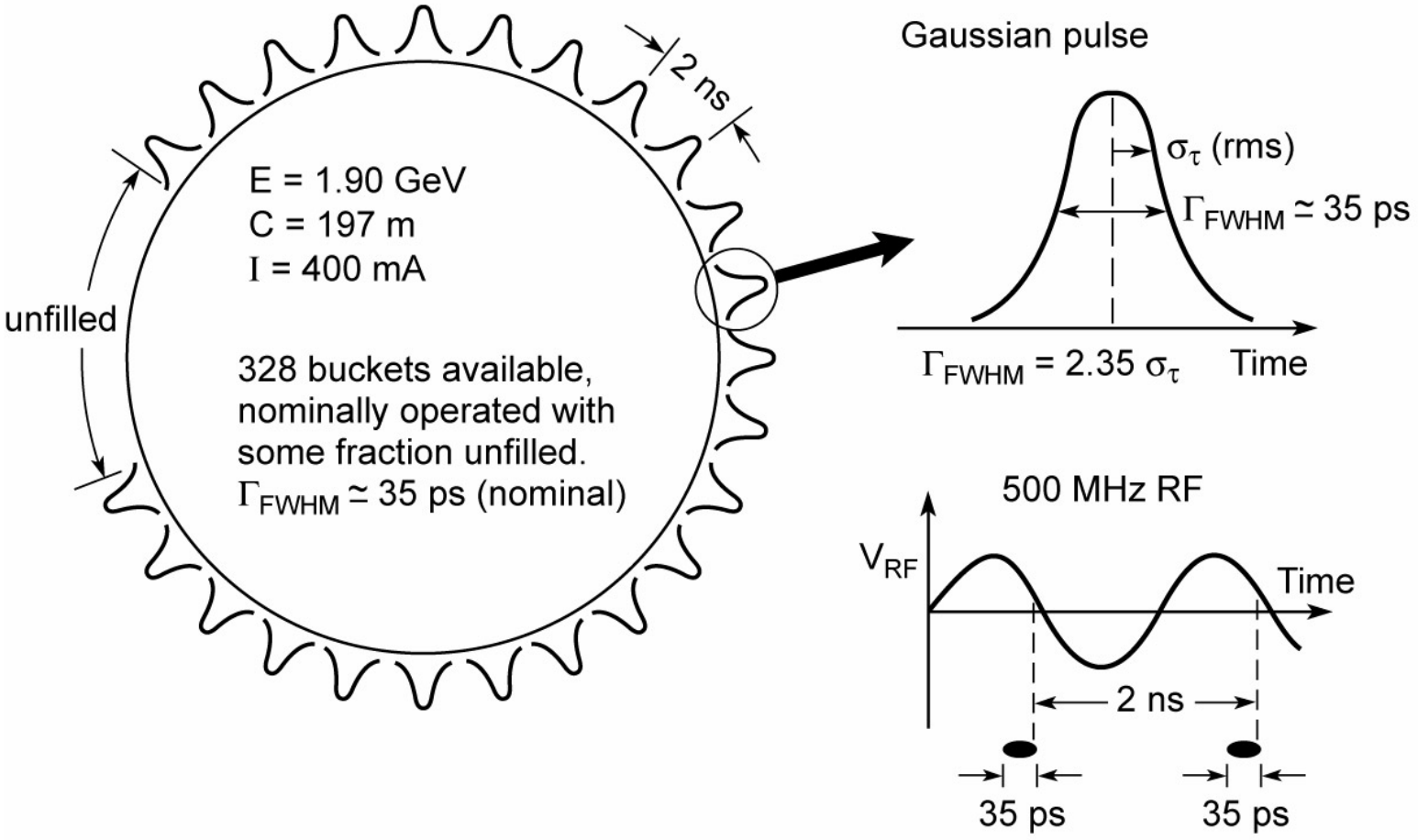

Ch05_TimeStruc.ai

Beamlines for spatially coherent undulator radiation

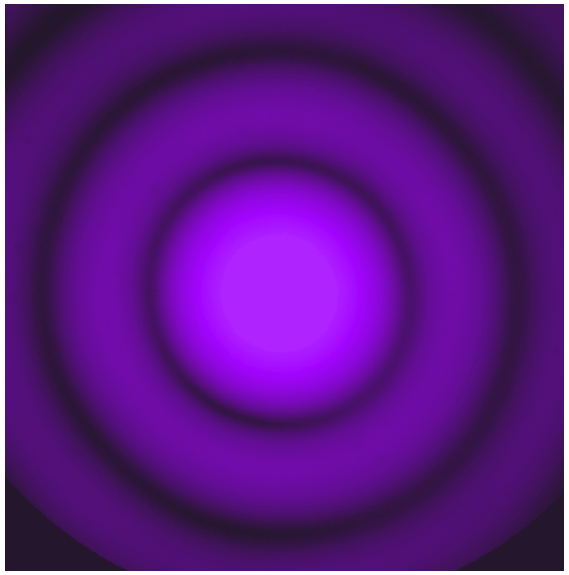

λ = 11.2 nm

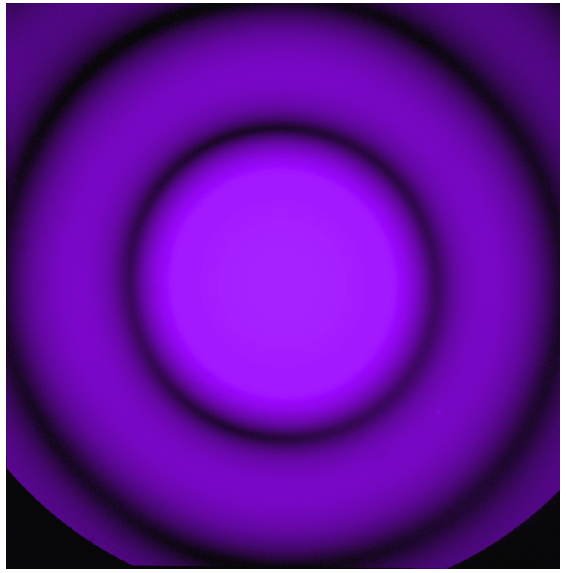

λ = 13.4 nm

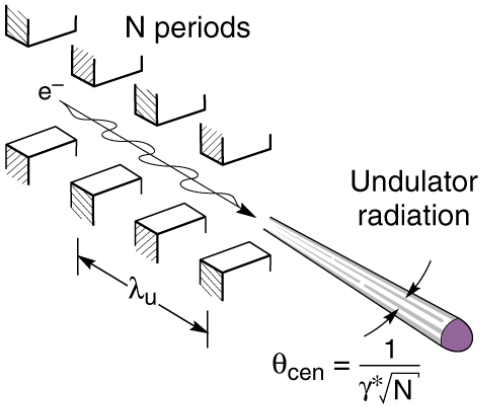

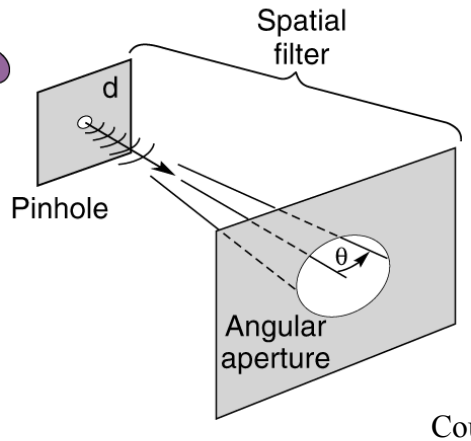

1 μm^D pinhole

25 mm wide CCD at 410 mm

Courtesy of Patrick Naulleau, LBNL.

Coherence at short wavelengths

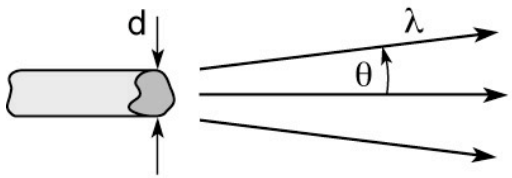

$$l_{coh} = \lambda^2/2\Delta\lambda \ \{\text{temporal (longitudinal) coherence}\} \quad (8.3)$$

$$d \cdot \theta = \lambda/2\pi \ \{\text{spatial (transverse) coherence}\} \quad (8.5)$$

$$\text{or } d \cdot 2\theta|_{FWHM} = 0.44\,\lambda \quad (8.5^*)$$

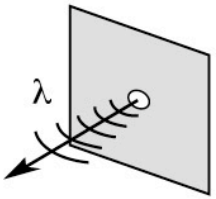

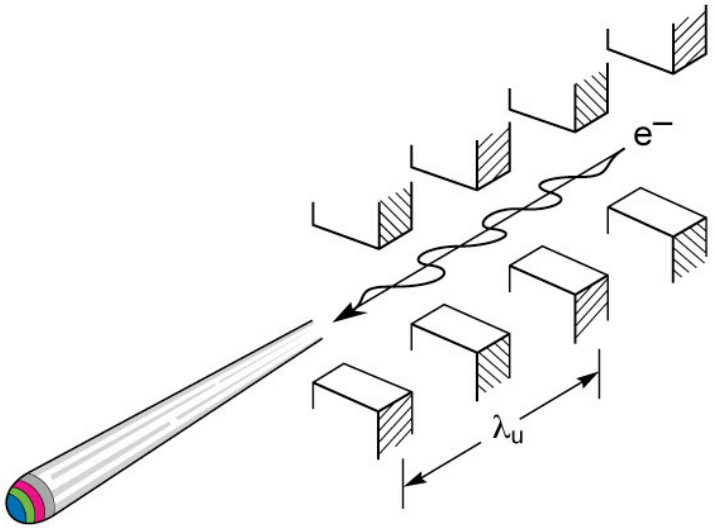

$$\bar{P}_{coh,N} = \frac{(\lambda/2\pi)^2}{(d_x\theta_x)(d_y\theta_y)}\bar{P}_{cen} \quad (8.6)$$

$$\bar{P}_{coh,\lambda/\Delta\lambda} = \frac{e\lambda_u I\eta(\Delta\lambda/\lambda)N^2}{8\pi\epsilon_0 d_x d_y} \cdot \left[1-\frac{\hbar\omega}{\hbar\omega_0}\right] f(K) \quad (8.9)$$

Ch08_F00_Sept2010.ai

Young's double slit experiment: spatial coherence and the persistence of fringes

Persistence of fringes as the source grows from a point source to finite size.

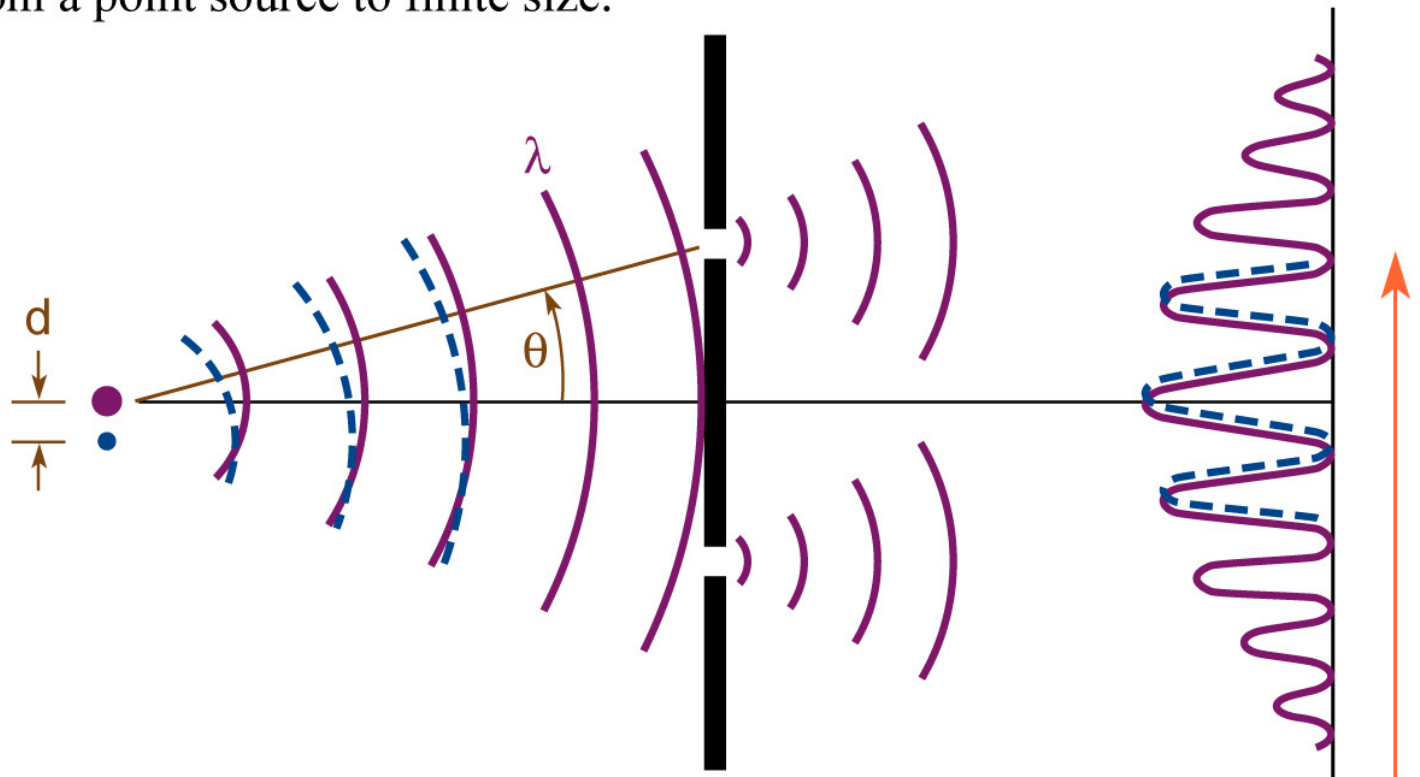

$$d \cdot 2\theta|_{FWHM} \simeq \lambda/2$$

$$\lambda_{coh} = \lambda^2/2\Delta\lambda = \frac{1}{2} N_{coh}\lambda$$

CH08_YoungsExprmt_v3.ai

Spatial and spectral filtering to produce coherent radiation

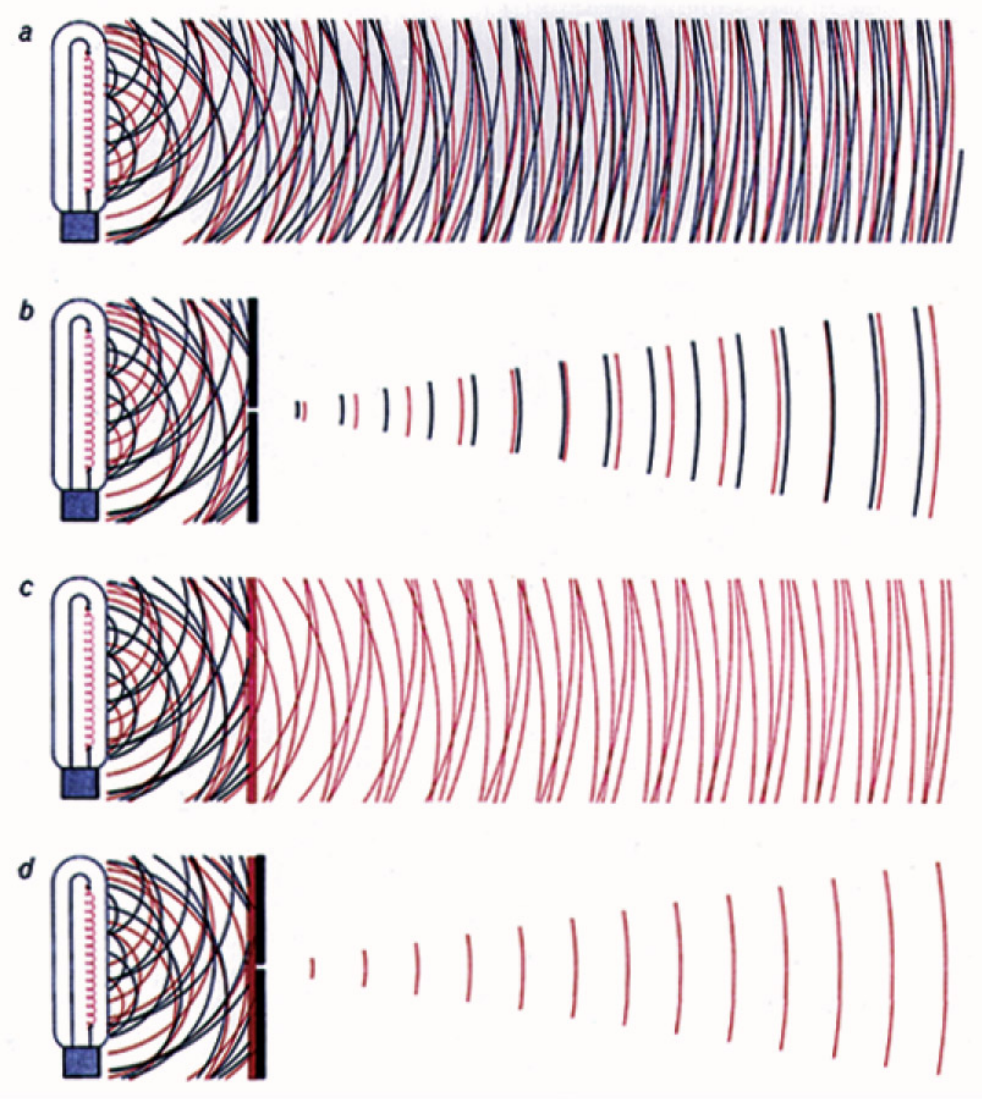

Courtesy of A. Schawlow, Stanford.

Ch08_F08.ai

Spatial and temporal coherence

Mutual coherence factor

$$\Gamma_{12}(\tau) \equiv \langle E_1(t+\tau)E_2^*(t)\rangle \qquad (8.1)$$

Normalize degree of spatial coherence (complex coherence factor)

$$\mu_{12} = \frac{\langle E_1(t)E_2^*(t)\rangle}{\sqrt{\langle|E_1|^2\rangle}\sqrt{\langle|E_2|^2\rangle}} \qquad (8.12)$$

A high degree of coherence ($\mu \to 1$) implies an ability to form a high contrast interference (fringe) pattern. A low degree of coherence ($\mu \to 0$) implies an absence of interference, except with great care. In general radiation is partially coherent.

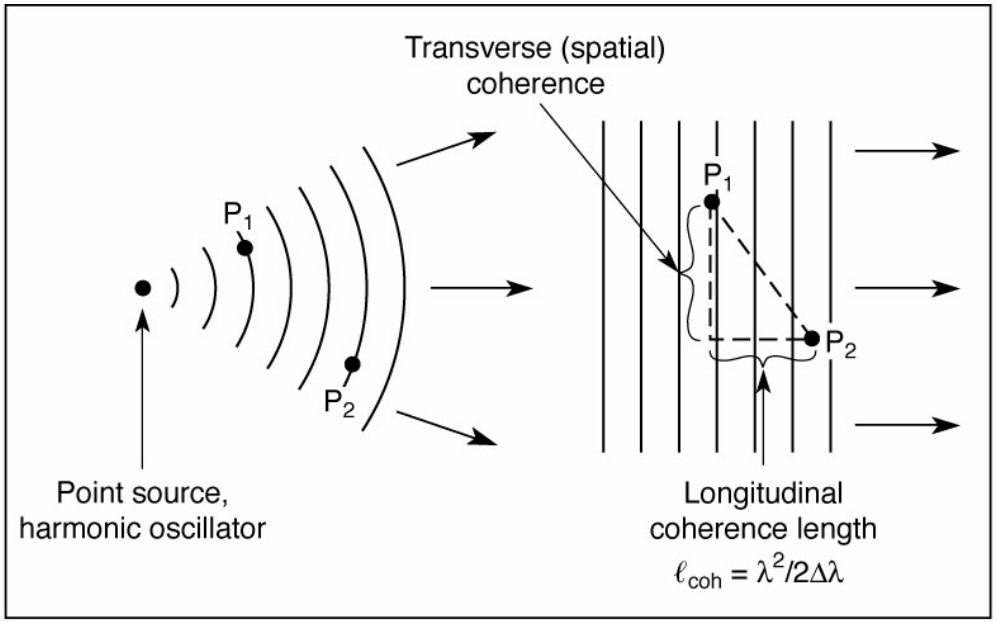

Longitudinal (temporal) coherence length

$$\ell_{coh} = \frac{\lambda^2}{2\,\Delta\lambda} \qquad (8.3)$$

Full spatial (transverse) coherence

$$d \cdot \theta = \lambda/2\pi \qquad (8.5)$$

Ch08_Eq1_12_F2.ai

Spatially filtered undulator radiation

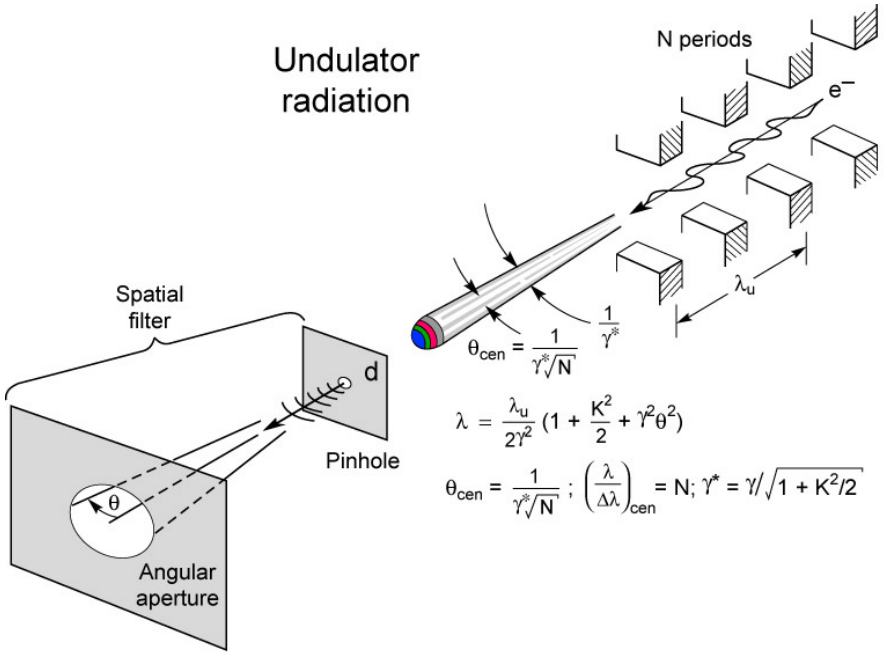

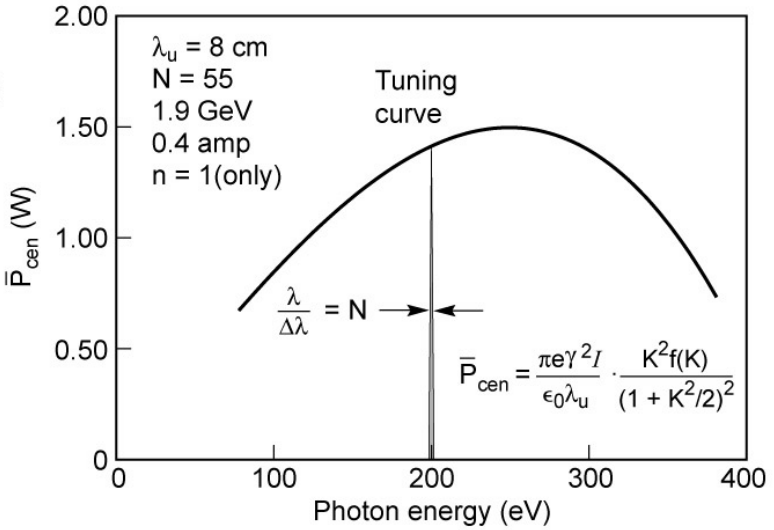

Using a pinhole-aperture spatial filter, passing only radiation that satisfies $d \cdot \theta = \lambda/2\pi$

$$\bar{P}_{coh,N} = \left(\frac{\lambda/2\pi}{d_x\theta_x}\right)\left(\frac{\lambda/2\pi}{d_y\theta_y}\right)\bar{P}_{cen} \qquad (8.6)$$

$$\bar{P}_{coh,N} = \frac{e\lambda_u I N}{8\pi\epsilon_0 d_x d_y}\left(1 - \frac{\hbar\omega}{\hbar\omega_0}\right) f(\hbar\omega/\hbar\omega_0) \qquad (8.9)$$

for $d_x = 2\sigma_x$, $d_y = 2\sigma_y$, $\theta_{Tx} \to \theta_x$, $\theta_{Ty} \to \theta_y$, and $\sigma'^2 << \theta_{cen}^2$.

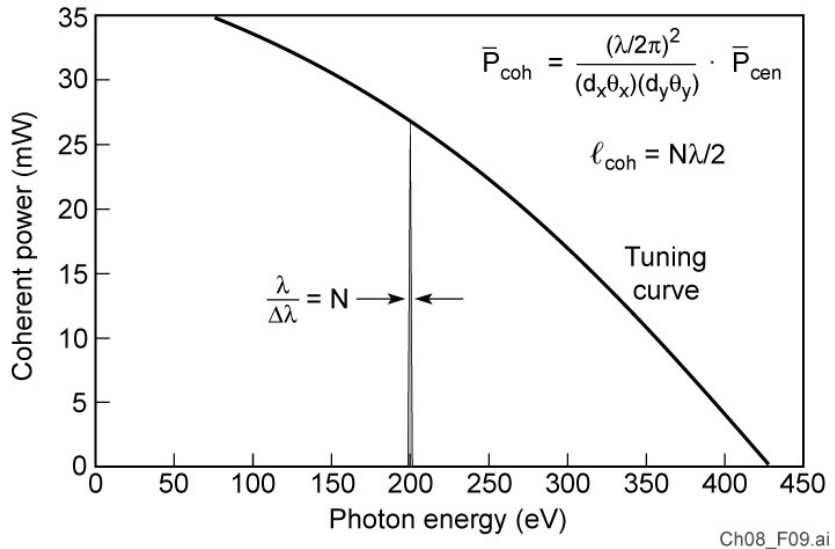

Ch08_F09.ai

Spatial and spectral filtering of undulator radiation

In addition to the pinhole – angular aperture for spatial filtering and spatial coherence, add a monochromator for narrowed bandwidth and increased temporal coherence:

$$\bar{P}_{\mathrm{coh},\lambda/\Delta\lambda} = \underbrace{\eta}_{\substack{\text{beamline}\\ \text{efficiency}}} \underbrace{\frac{(\lambda/2\pi)^2}{(d_x\theta_x)(d_y,\theta_y)}}_{\substack{\text{spatial}\\ \text{filtering}}} \cdot \underbrace{N\frac{\Delta\lambda}{\lambda}}_{\substack{\text{spectral}\\ \text{filtering}}} \cdot \bar{P}_{\mathrm{cen}} \qquad (8.10a)$$

which for $\sigma'^{2}_{x,y} << \theta^{2}_{\mathrm{cen}}$ (the undulator condition) gives the spatially and temporally coherent power ($d \cdot \theta = \lambda/2\pi$; $l_{\mathrm{coh}} = \dfrac{\lambda^2}{2\,\Delta\lambda}$)

$$\bar{P}_{\mathrm{coh},\lambda/\Delta\lambda} = \frac{e\lambda_u I \eta(\Delta\lambda/\lambda)N^2}{8\pi\epsilon_0 d_x d_y} \cdot \left(1 - \frac{\hbar\omega}{\hbar\omega_0}\right) f(\hbar\omega/\hbar\omega_0) \qquad (8.10c)$$

which we note scales as N^2.

Ch08_SpatialSpectral.ai

Spatially and spectrally filtered undulator radiation

- Pinhole filtering for full spatial coherence
- Monochromator for spectral filtering to $\lambda/\Delta\lambda > N$

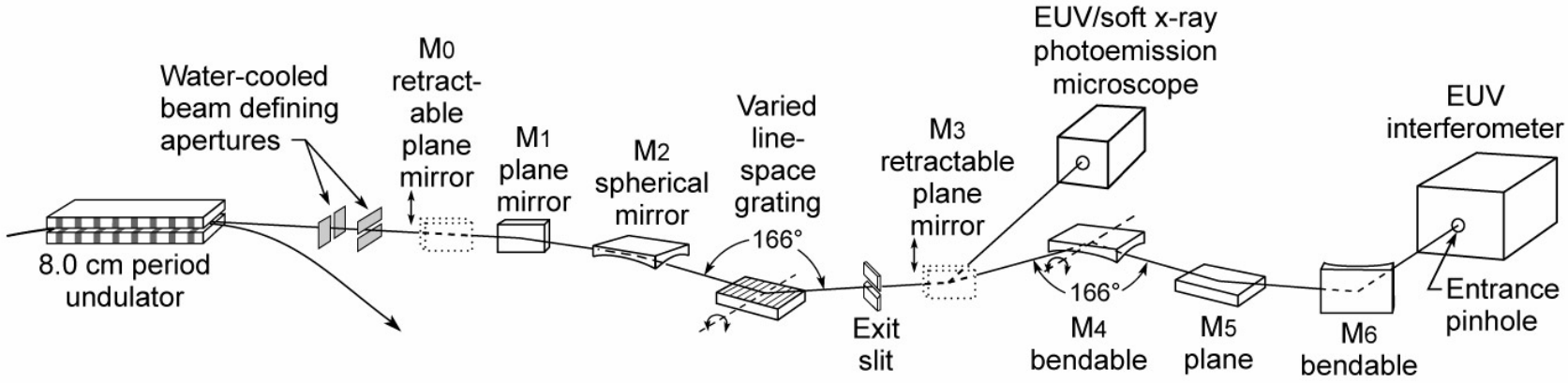

$$\bar{P}_{\mathrm{coh},\lambda/\Delta\lambda} = \underbrace{\eta}_{\substack{\text{beamline}\\ \text{efficiency}}} \underbrace{\frac{(\lambda/2\pi)^2}{(d_x\theta_x)(d_y\theta_y)}}_{\substack{\text{spatial}\\ \text{filtering}}} \cdot \underbrace{N\frac{\Delta\lambda}{\lambda}}_{\substack{\text{spectral}\\ \text{filtering}}} \cdot \bar{P}_{\mathrm{cen}} \qquad (8.10a)$$

$$\bar{P}_{\mathrm{coh},\lambda/\Delta\lambda} = \frac{e\lambda_u I\eta(\Delta\lambda/\lambda)N^2}{8\pi\epsilon_0 d_x d_y} \cdot \left(1 - \frac{\hbar\omega}{\hbar\omega_0}\right) f(\hbar\omega/\hbar\omega_0)$$

$$\left(\sigma'^2 \ll \theta_{\mathrm{cen}}^2\right) \qquad (8.10c)$$

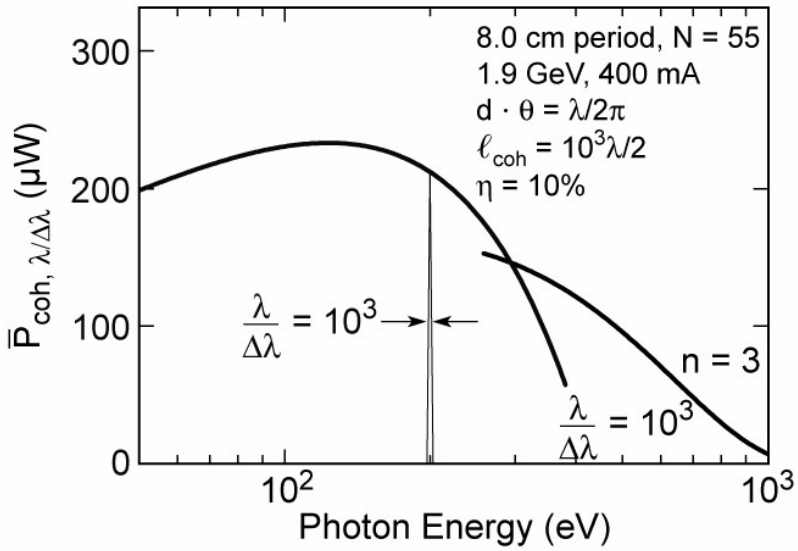

Ch08_F11_Mar08.ai

Coherent soft x-ray science beamline

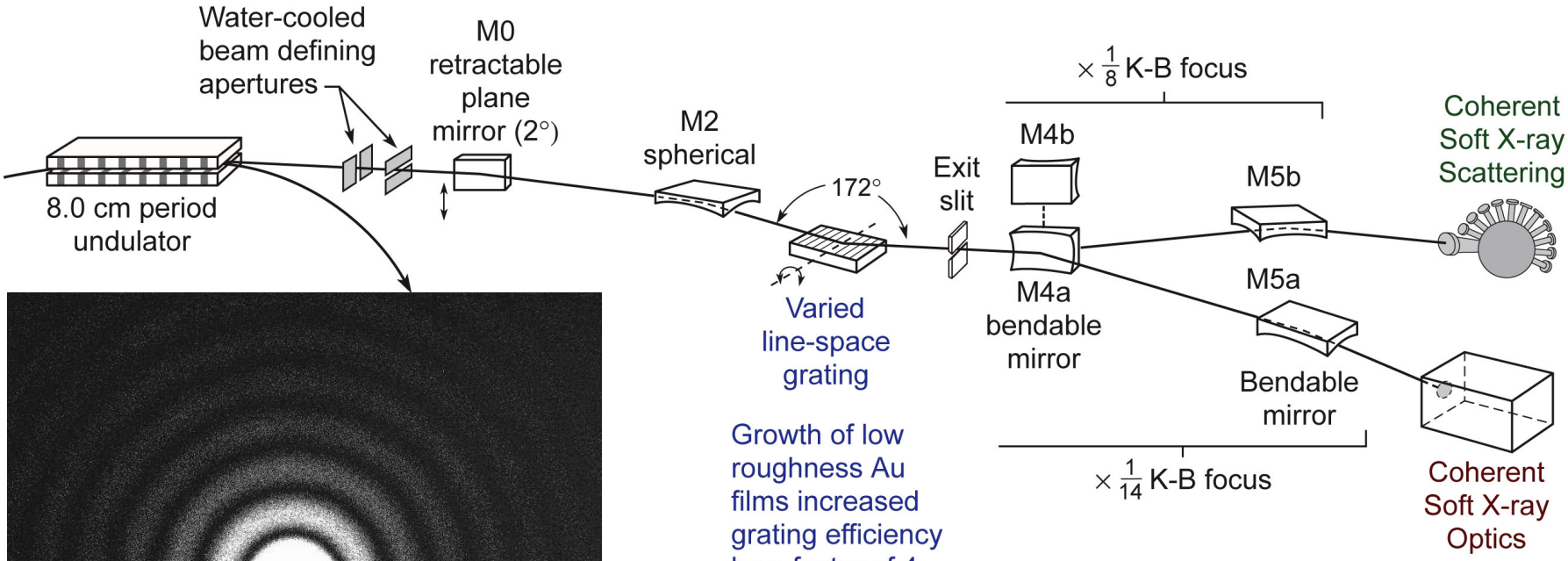

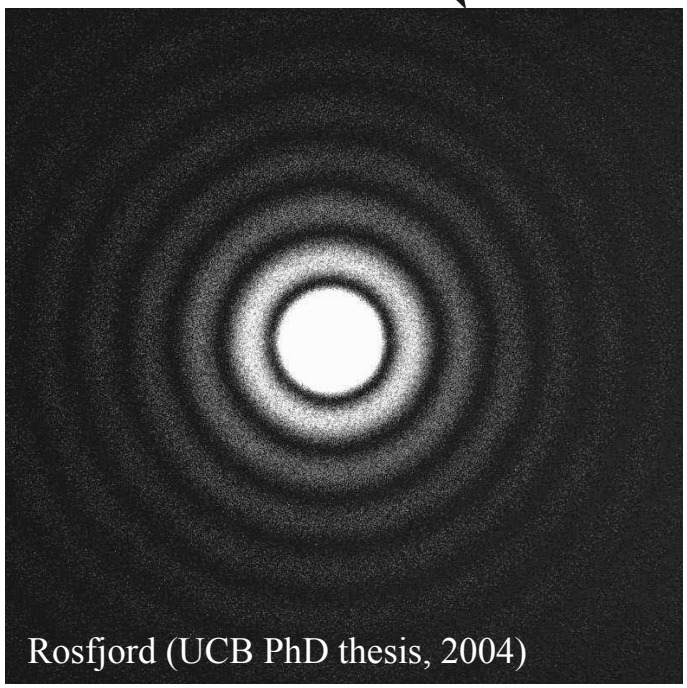

K. Rosfjord, Y. Liu, D. Attwood, "Tunable Coherent Soft X-Rays", IEEE J. Sel. Top. Quant. Electr.**10**, 1405 (Nov/Dec 2004)

Energy range 200-1000eV

Coherent flux at 600 eV:
2×10^{11} ph/sec/0.1%BW

λ = 2.07 nm (600 eV)

- Wavefront interferomery to measure aberrations in zone plate lenses
- Measure material properties (f_1 & f_2)
- Develop new coherent soft x-ray optical techniques (Fourier Optics)
- Coherent scattering from magnetic nanostructures

Undulator beamline for high spatial coherence measurements

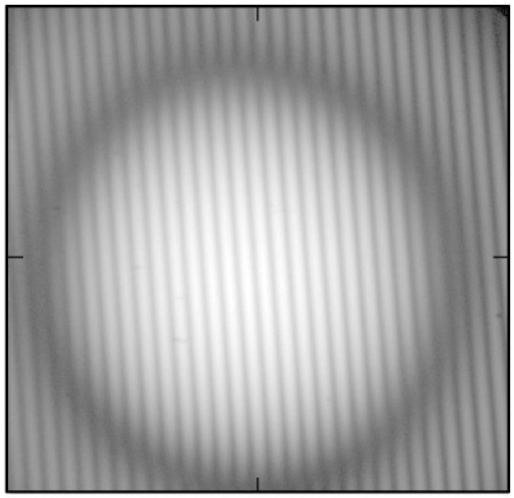

C. Chang

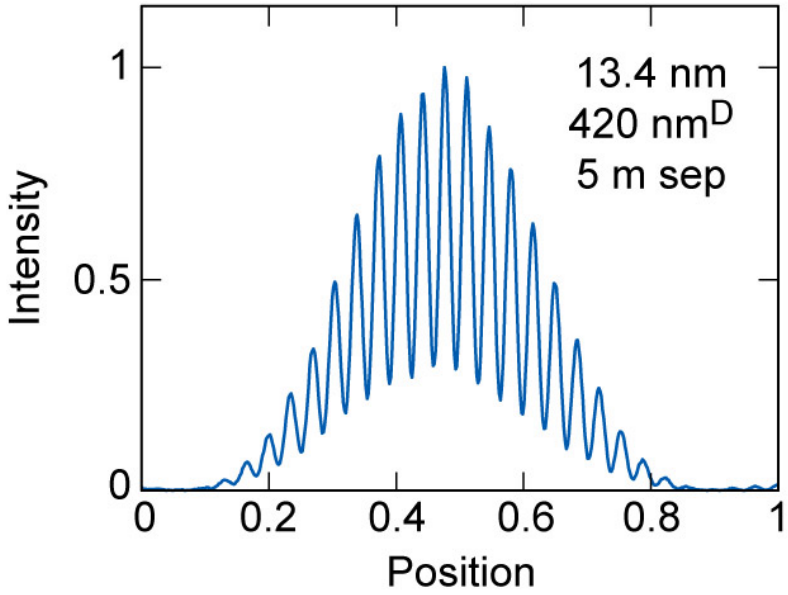

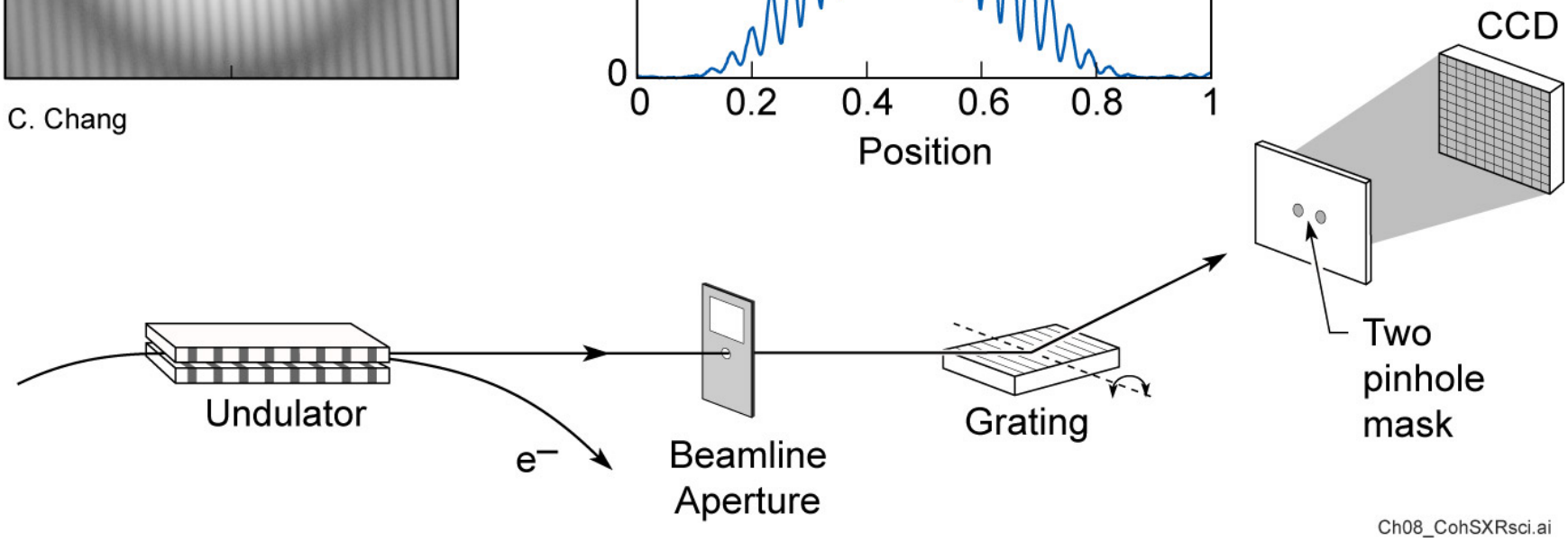

Spatial coherence measurements of undulator radiation using the classic 2-pinhole technique

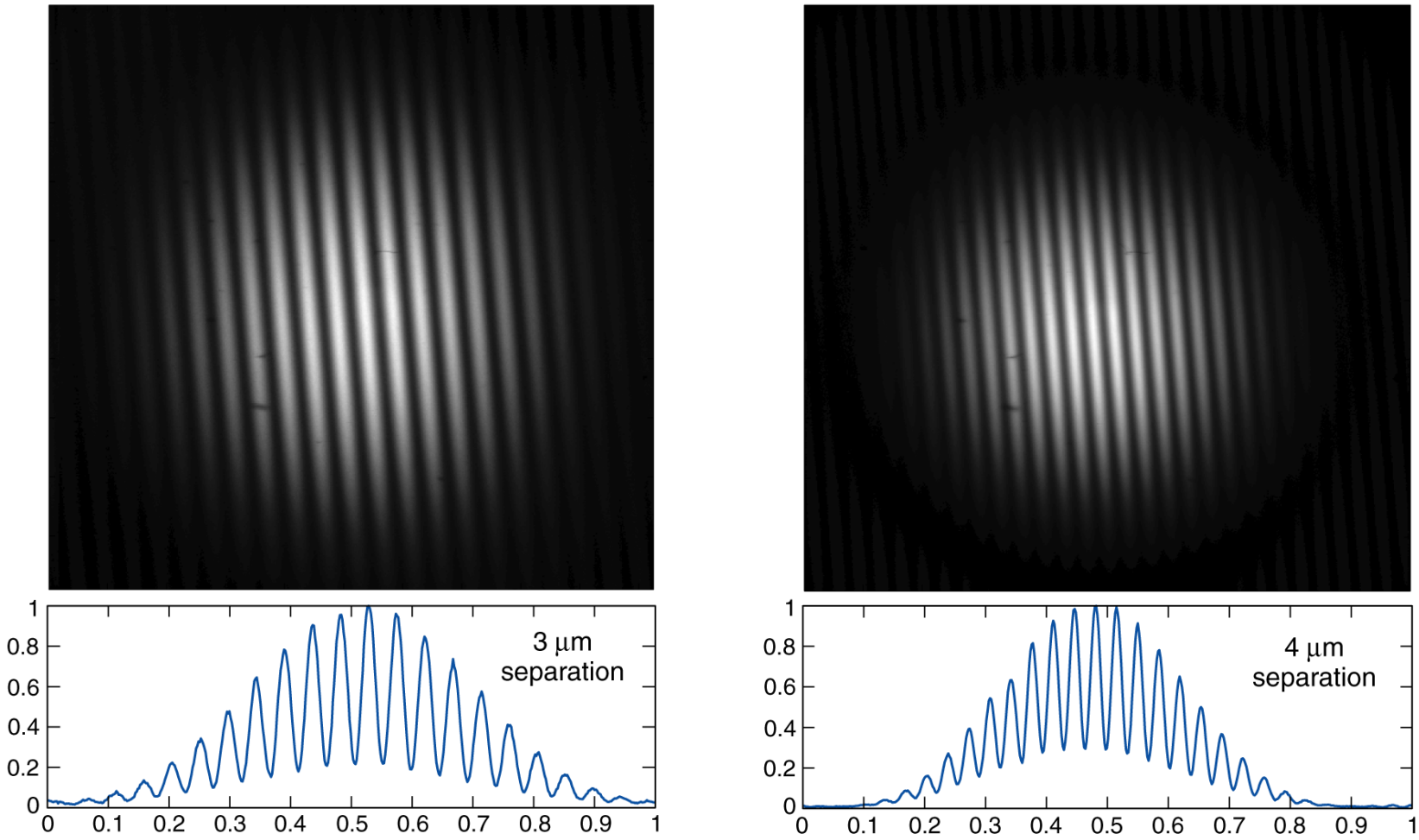

Courtesy of Chang Chang, UC Berkeley and LBNL.

λ = 13.4 nm, 450 nm diameter pinholes, 1024 x 1024 EUV/CCD at 26 cm ALS, 1.9 GeV, λ_u = 8 cm, N = 55

Spatial coherence measurements of undulator radiation using the classic 2-pinhole technique

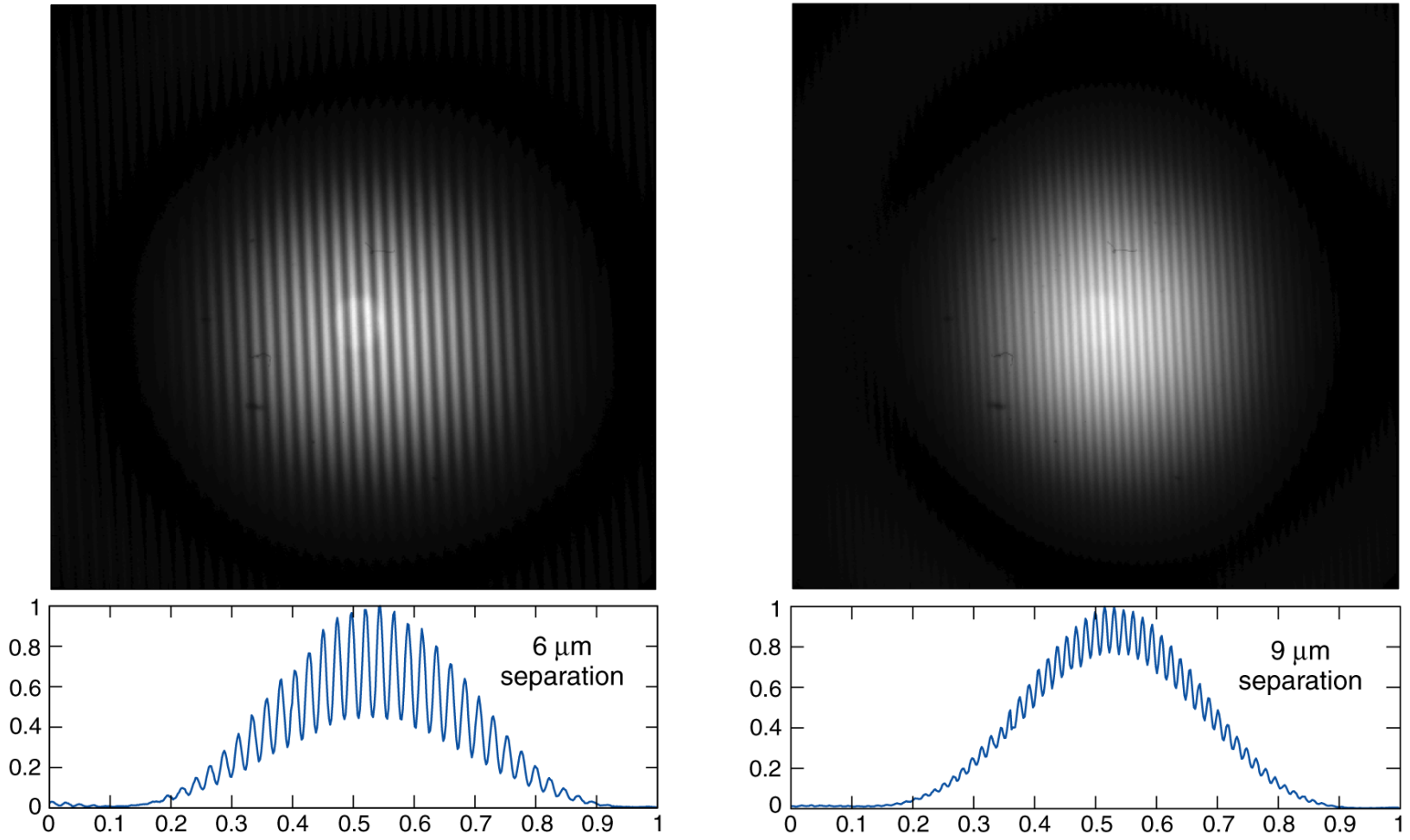

Courtesy of Chang Chang, UC Berkeley and LBNL.

λ = 13.4 nm, 450 nm diameter pinholes, 1024 x 1024 EUV/CCD at 26 cm ALS, 1.9 GeV, λ_u = 8 cm, N = 55

Coherent power for an EPU at the ALS

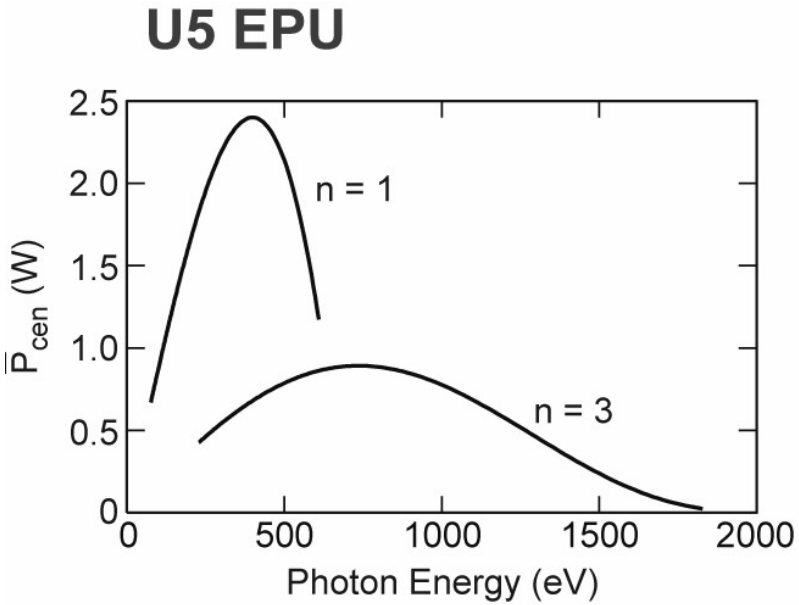

1.9 GeV, 400 mA

λ_u = 50 mm, N = 27

$0.5 \le K \le 4.0$

σ_x = 260 μm, σ_x' = 23 μr

σ_y = 16 μm, σ_y' = 3.9 μr

θ_{cen} = 61μr @ K = 0.87 (500 eV)

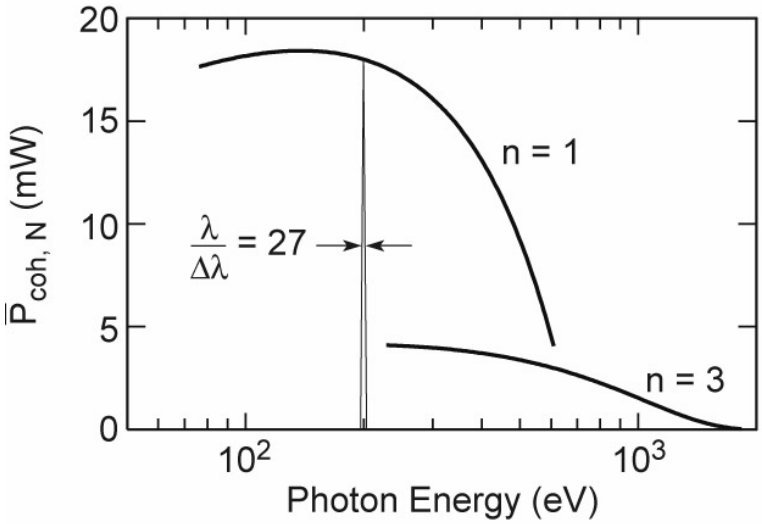

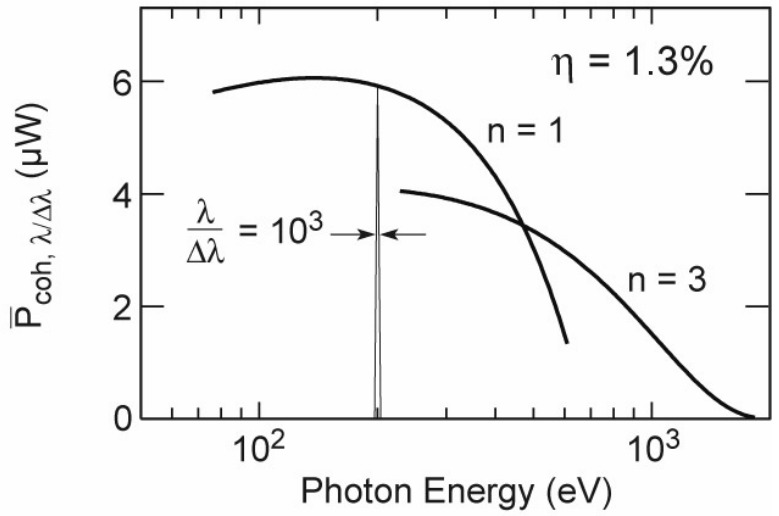

Ch08_ALS_U5epu_Feb07.ai

Coherent power at the Australian Synchrotron

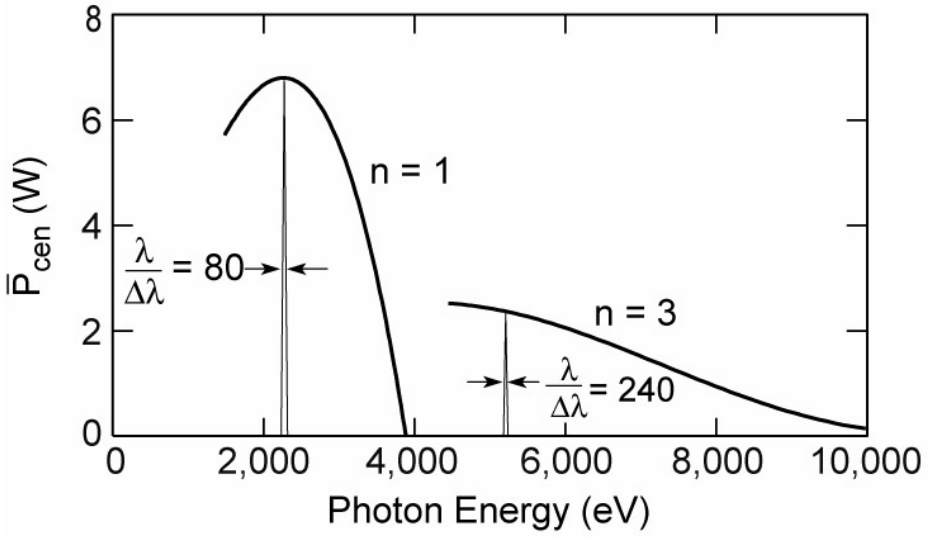

3.0 GeV, 200 mA
λ_u = 22 mm, N = 80
$0 \le K \le 1.8$
σ_x = 320 μm, σ_x' = 34 μrad
σ_y = 16 μm, σ_y' = 6 μrad
θ_{cen} = 23 μrad @ K = 1
η = 10%

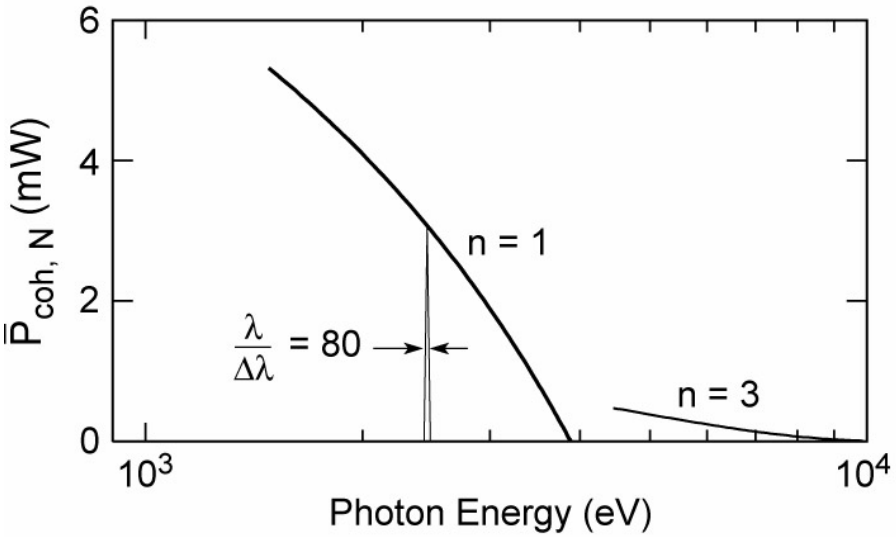

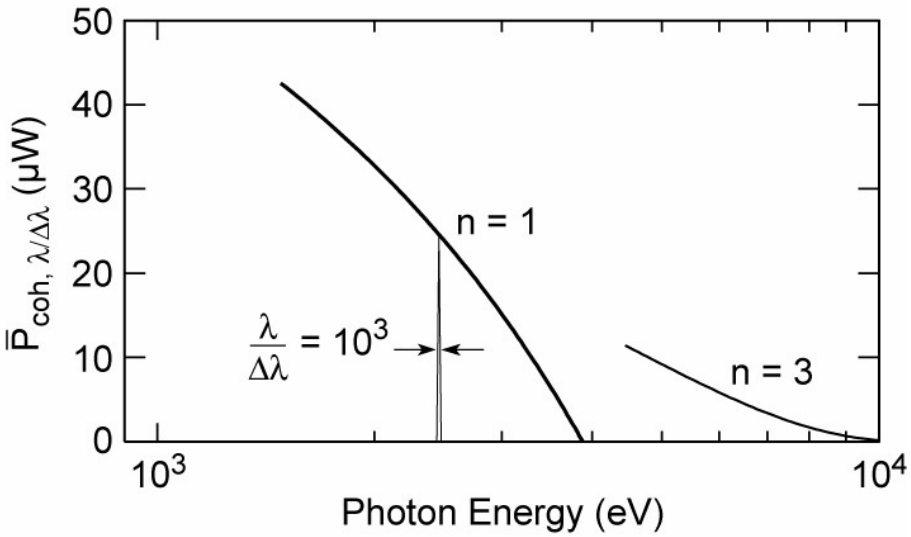

CohPwr_AustralSynch_Feb07.ai

Coherent power at SPring-8

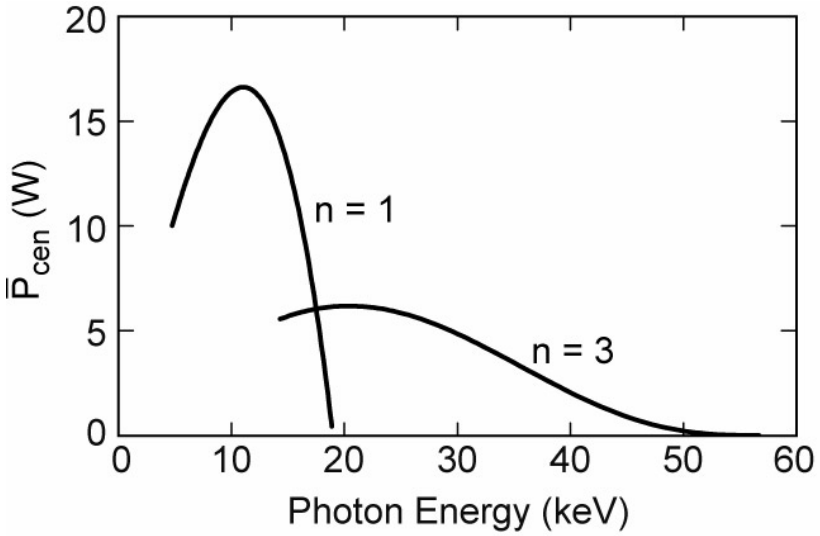

8 GeV, 100 mA
λ_u = 32 mm, N = 140
$0 \leq K \leq 2.46$
σ_x = 393 μm, σ_x' = 15.7 μr
σ_y = 4.98 μm, σ_y' = 1.24 μr
η = 10%

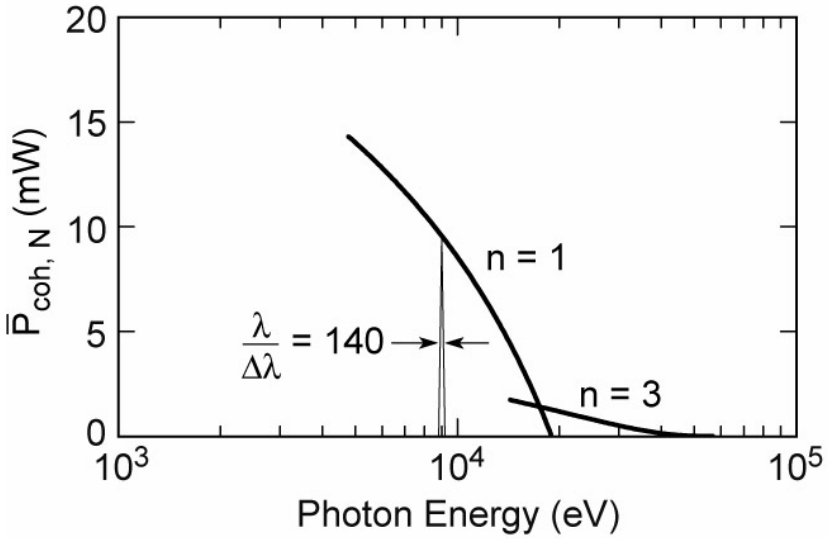

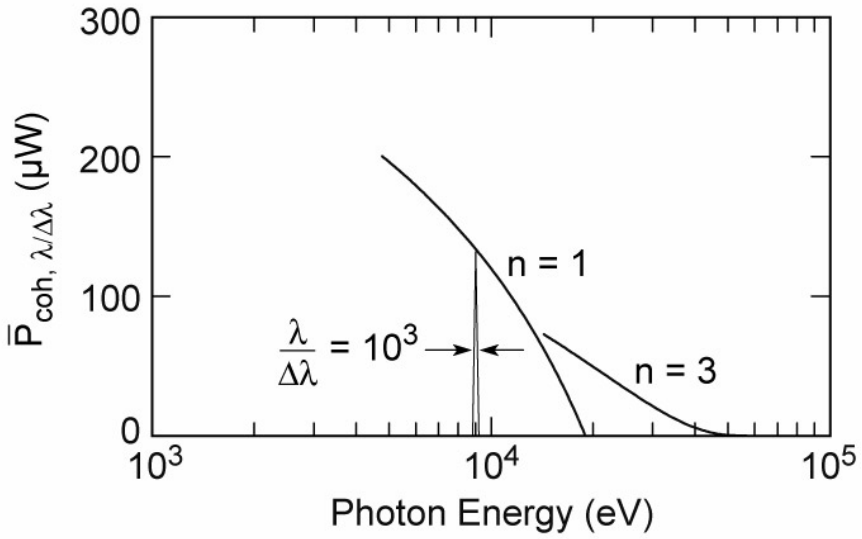

Ch08_SPring8_Feb07.ai

Coherent soft x-ray beamline: use of a higher harmonic (n = 3) to access shorter wavelengths

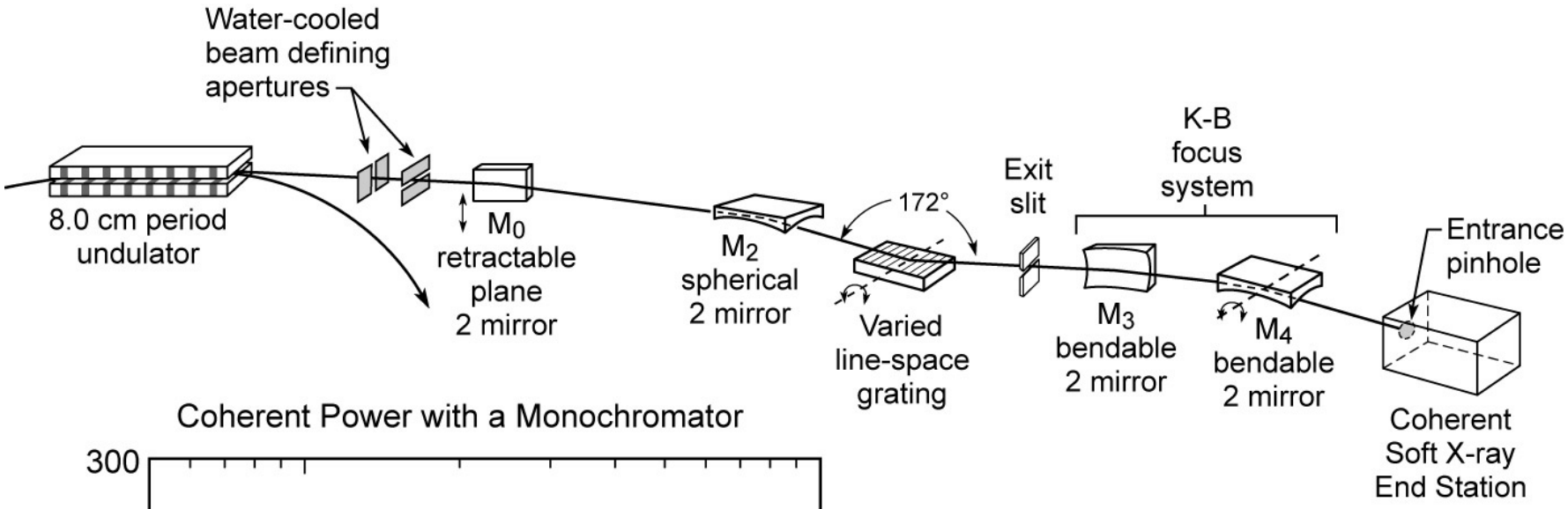

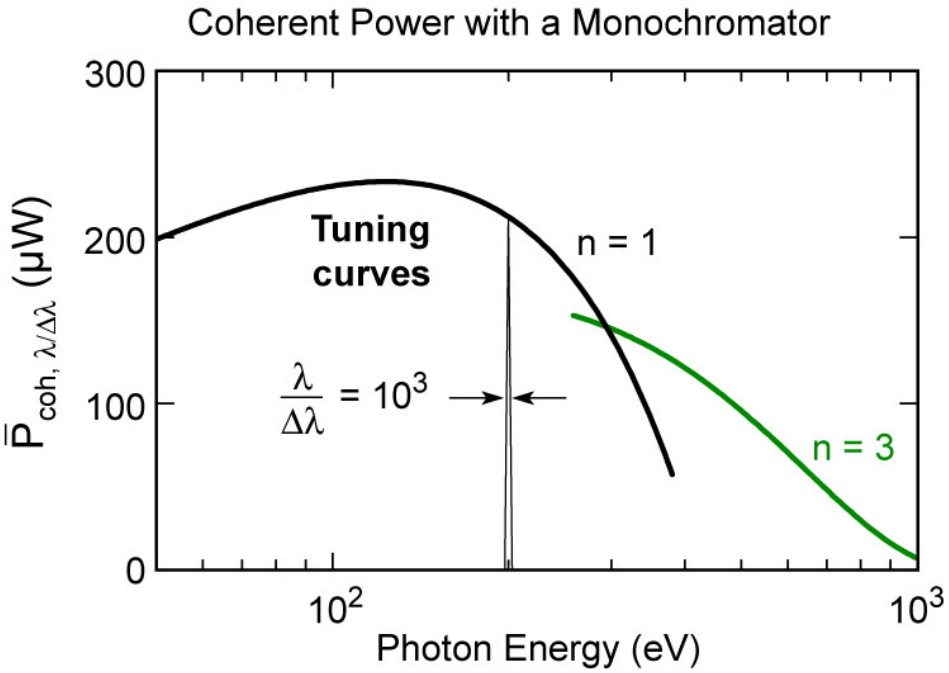

8.0 cm period, N = 55
1.9 GeV, 400 mA
$d \cdot \theta = \lambda/2\pi$
$\ell_{coh} = 1000\ \lambda/2$
$\eta_{euv} = 10\%$, $\eta_{sxr} = 10\%$

Ch08_CohOptBLwGraf_Feb07.ai

Coherent Soft X-Ray Magnetic Scattering Endstation

Flangosaurus

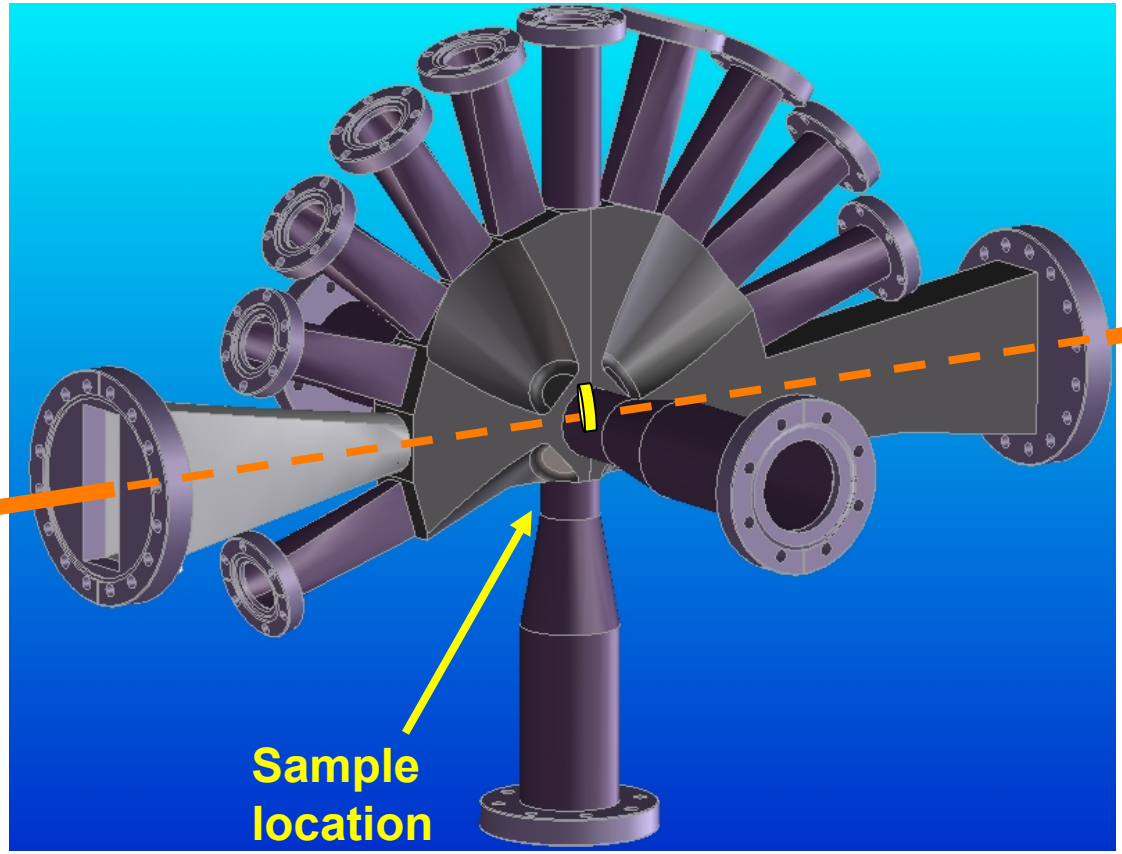

Courtesy of K.Chesnel, S. Kevan, U. Oregon

Example of experiment in transmission: coherent scattering from nanoparticles

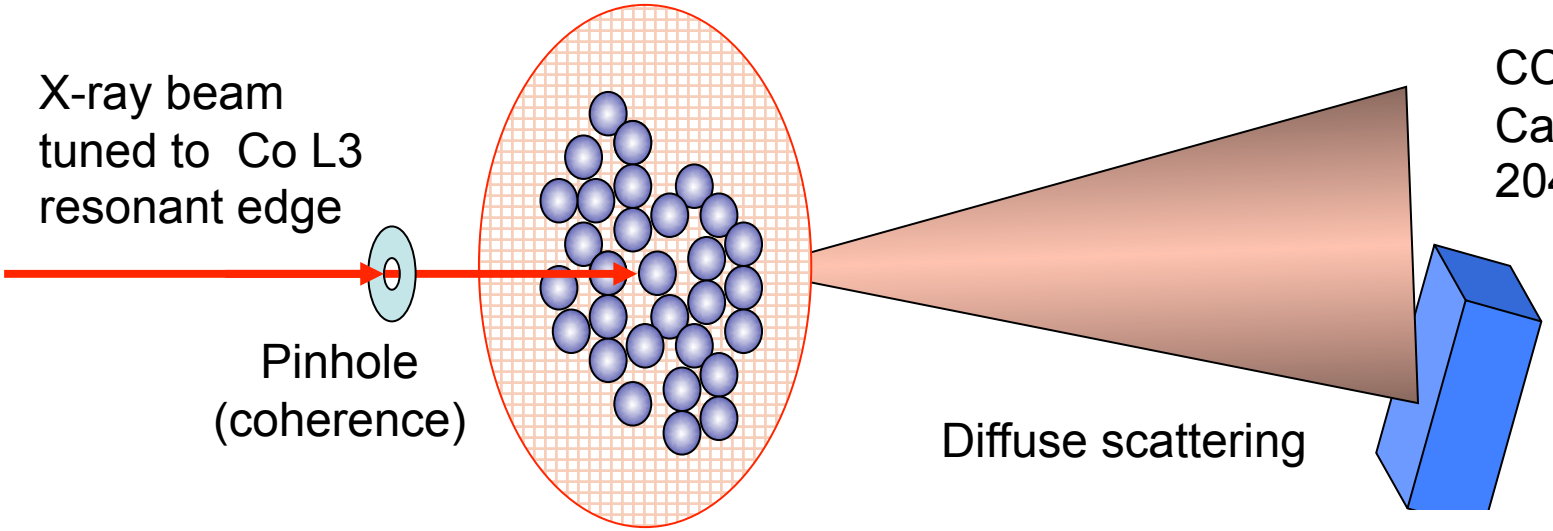

Co Nanoparticles assembly precipitated on TEM grid

Scattering ring related to interparticle distance ~12 nm

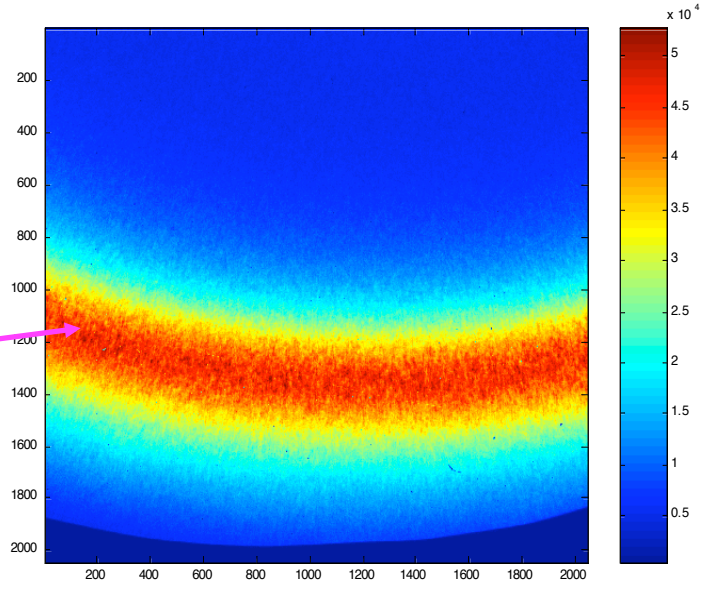

Courtesy of K.Chesnel, S. Kevan, U. Oregon


16 December 2004
International weekly journal of science
nature
$10.00
www.nature.com/nature
Inside this week
nature insight
chemical space
X-ray holography
Lensless imaging at the nanoscale
The 'Halloween storm'
How the Sun plays its tricks
Protein transport
Escape from the nucleus
Duck-billed platypus
Curiouser and curiouser
Locusts over Africa
Time for biological control?
$10.00US $12.99CAN

Coherent power at BESSY II

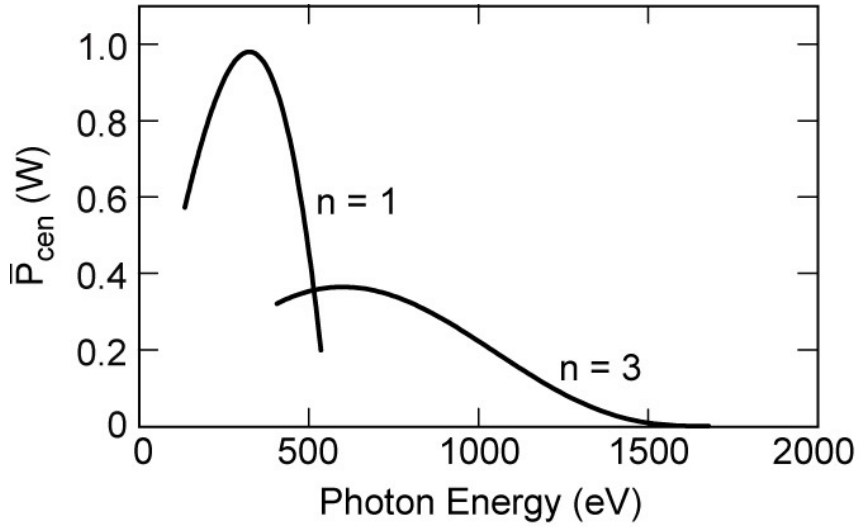

1.7 GeV, 200 mA
λ_u = 49 mm, N = 84
$0 \le K \le 2.5$
σ_x = 314 μm, σ_x' = 18 μr
σ_y = 24 μm, σ_y' = 2 μr
η_{euv} = 10% ; η_{sxr} = 10%

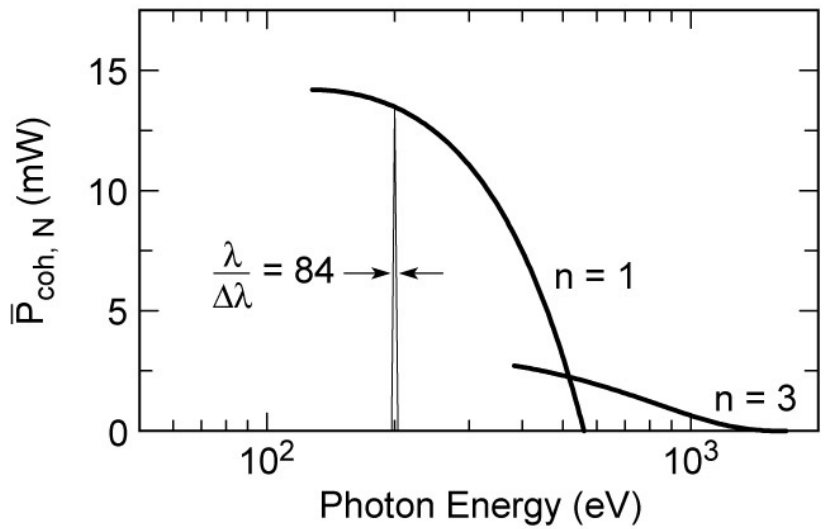

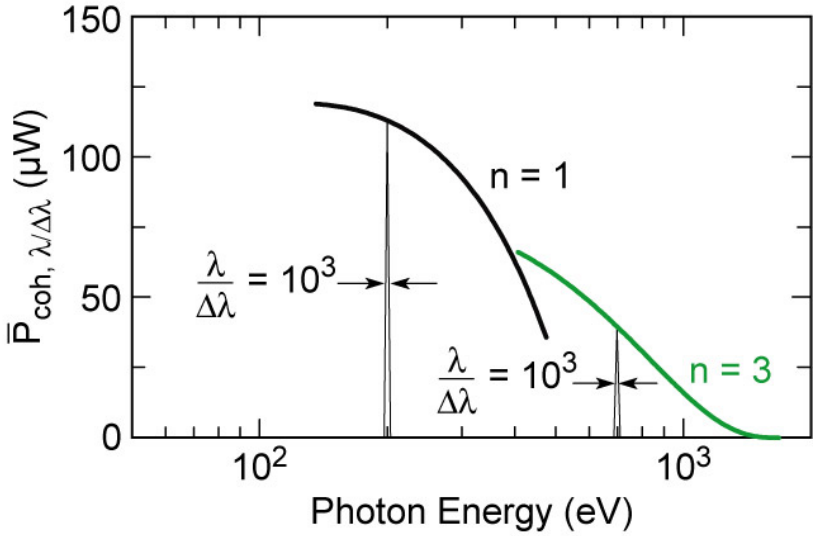

Ch08_BESSYII_Nov07.ai

Lensless imaging of magnetic nanostructures by x-ray spectro-holography

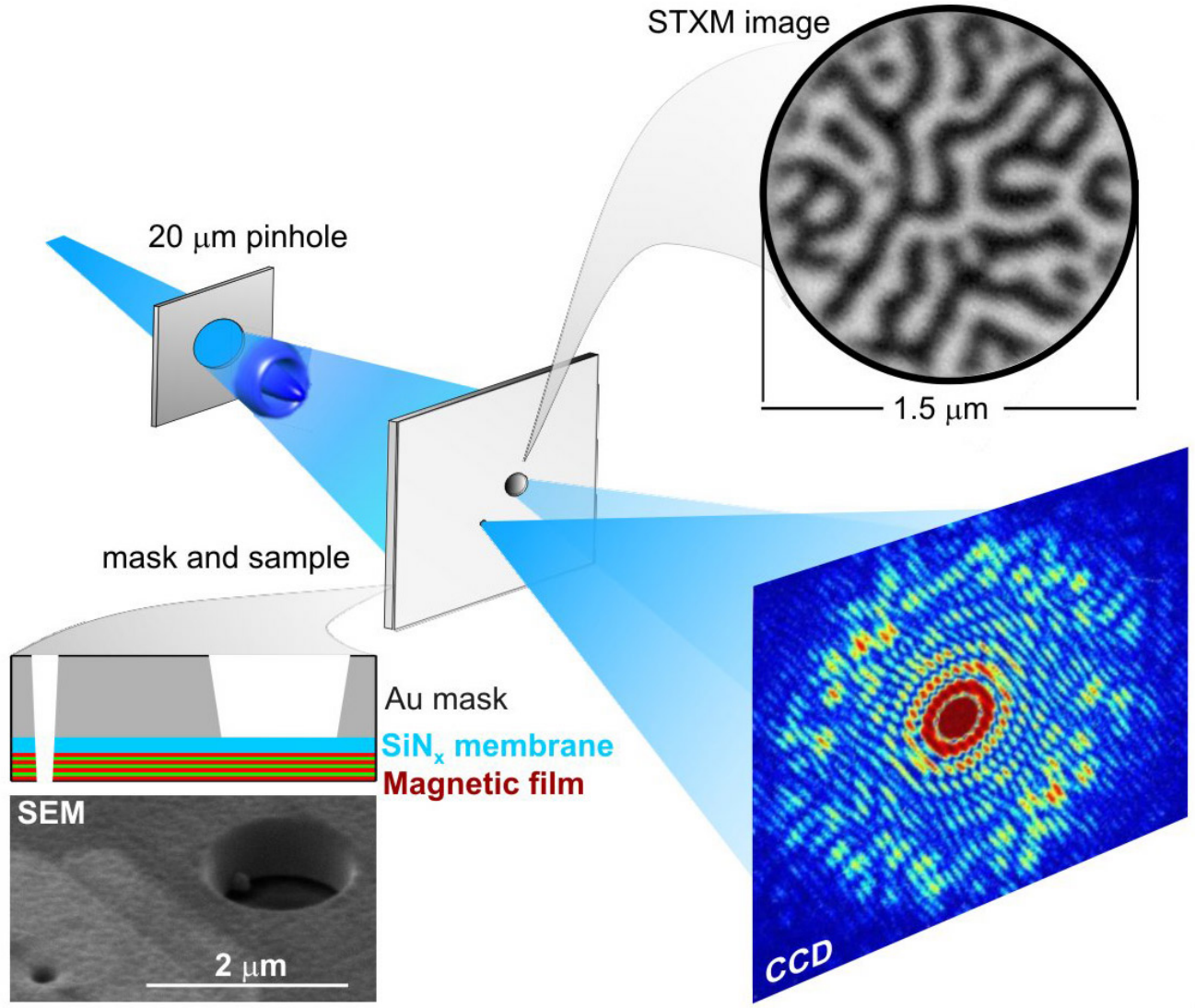

S. Eisebitt, J. Lüning, W.F. Schlotter, M. Lörgen, O. Hellwig, W. Eberhardt & J. Stöhr / *Nature*, 16 Dec 2004

LenslessImagingF1.ai

Undulators, FELs and coherence

- Spatial coherence
- Temporal coherence
- Partial coherence
- Full coherence
- Spatial filtering
- Uncorrelated emitters
- Correlated emitters
- True phase coherence and mode control
- Lasers, amplified spontaneous emission (ASE) and mode control
- Undulator radiation
- SASE FEL 100^{+} fsec soft/hard x-rays
- Seeded FEL true phase coherent x-rays
- High harmonic generation (HHG) compact fsec/asec EUV
- EUV lasers and laser seeded HHG
- Applications with uncorrelated emitters
- Applications with correlated emitters

FEL Physics

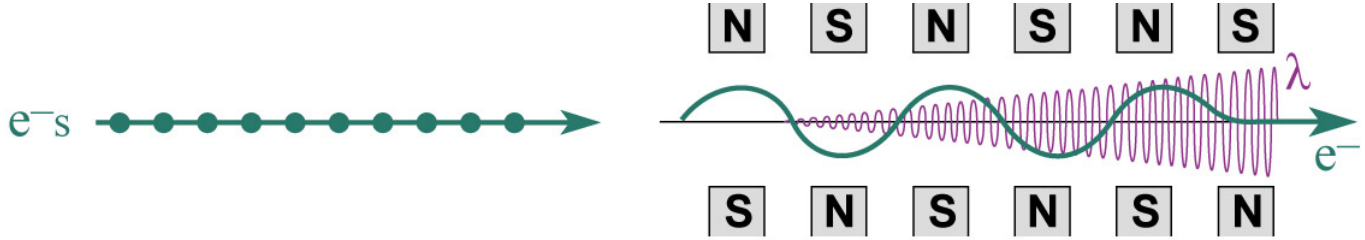

- Uniformly distributed particles (beam) into undulator.
- Emission of radiation ("spontaneous" emission).
- Wave grows enough (undulator radiation) to begin affecting. particle dynamics through $m\mathbf{a} = -e\mathbf{E}$ radiation.
- Transverse coupling between $\mathbf{E}_{rad}$ and transverse velocity $\mathbf{v}_x$ (in undulator) leads to energy exchange between fields and particle (zero net at first) $\frac{dEe}{dt} = mc^2 \frac{d\gamma}{dt} = \mathbf{F} \cdot \mathbf{v} = -e\, E \cdot \mathbf{v}_x$
- Modulated velocities with increments in $\mathbf{v}_x$ lead to bunching on axis.
- Electron density modulation leads to stronger radiation,

$$P_{rad} \propto q^2|a|^2 \sim (eN_e)^2 \cdot \frac{e^2}{m^2} = N_e^2 \frac{e^4}{m^2}$$

- Stronger fields (wave) drive stronger transverse velocity.
- Stronger $\mathbf{v}_x$ drives stronger bunching, . . . stronger fields, . . . FEL action.

Young's double slit experiment: spatial coherence and the persistence of fringes

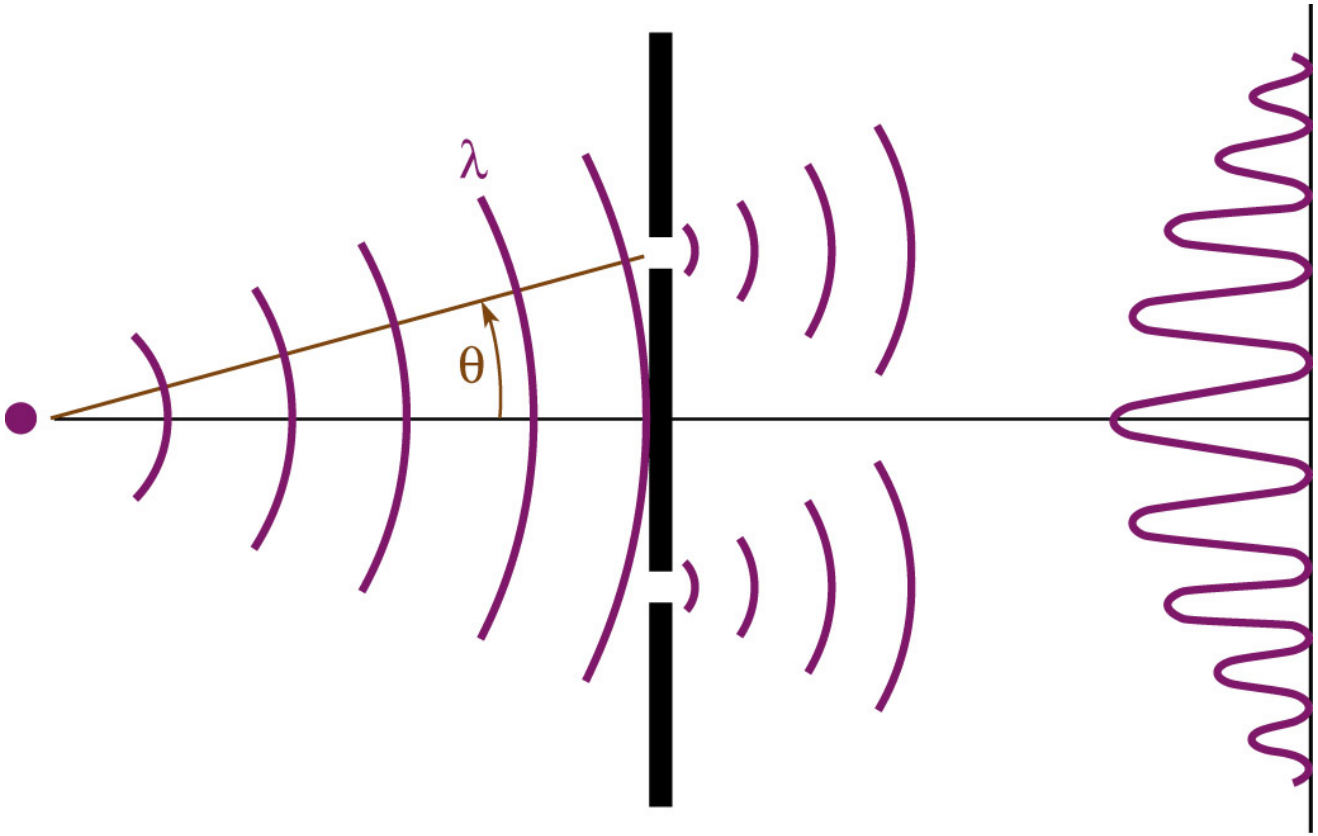

YoungsExprmt.ai

Young's double slit experiment: spatial coherence and the persistence of fringes

Persistence of fringes as the source grows from a point source to finite size.

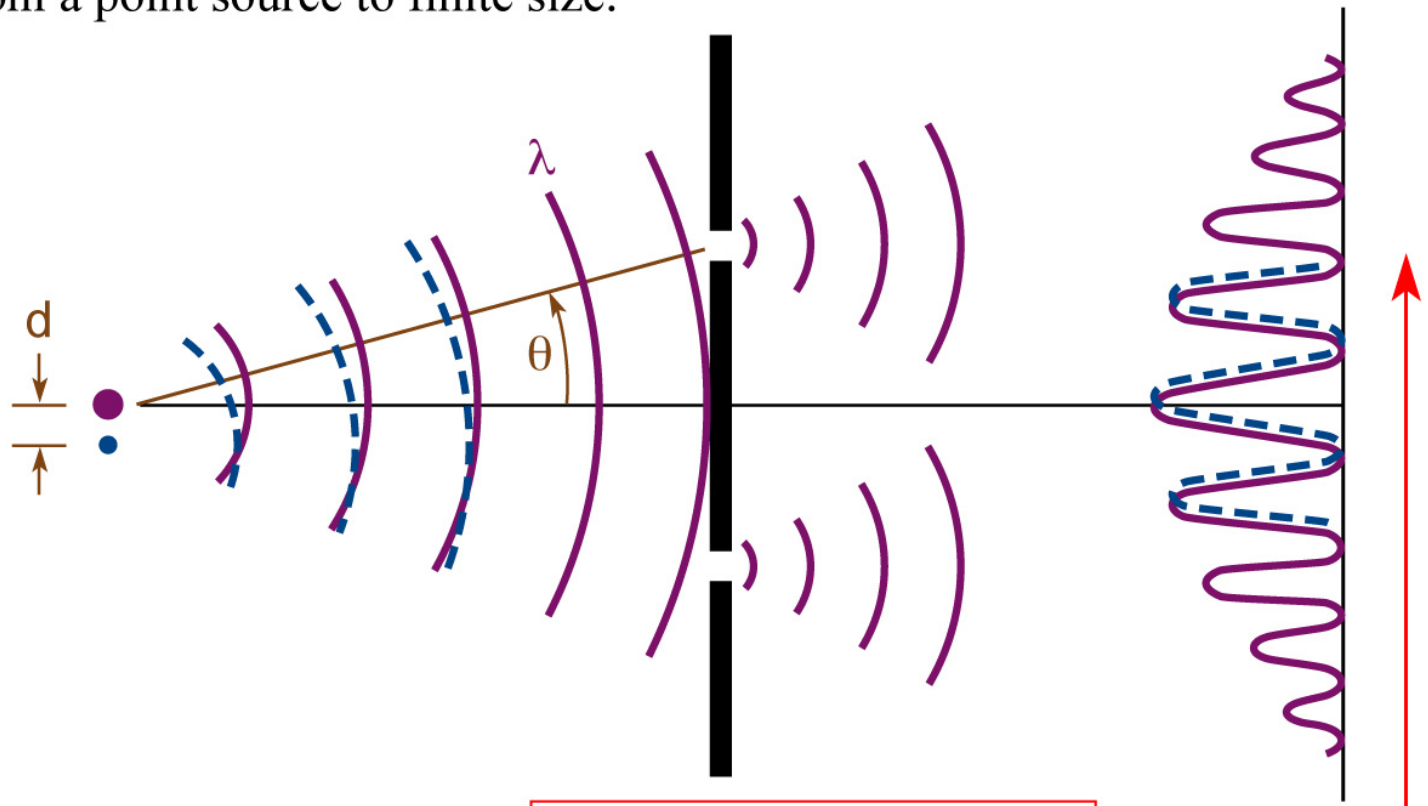

$$d \cdot 2\theta|_{FWHM} \simeq \lambda/2$$

$$\lambda_{coh} = \lambda^2/2\Delta\lambda = \frac{1}{2} N_{coh}\lambda$$

CH08_YoungsExprmt_v3_Sept2011.ai

Young's double slit experiment with random emitters: Young did not have a laser

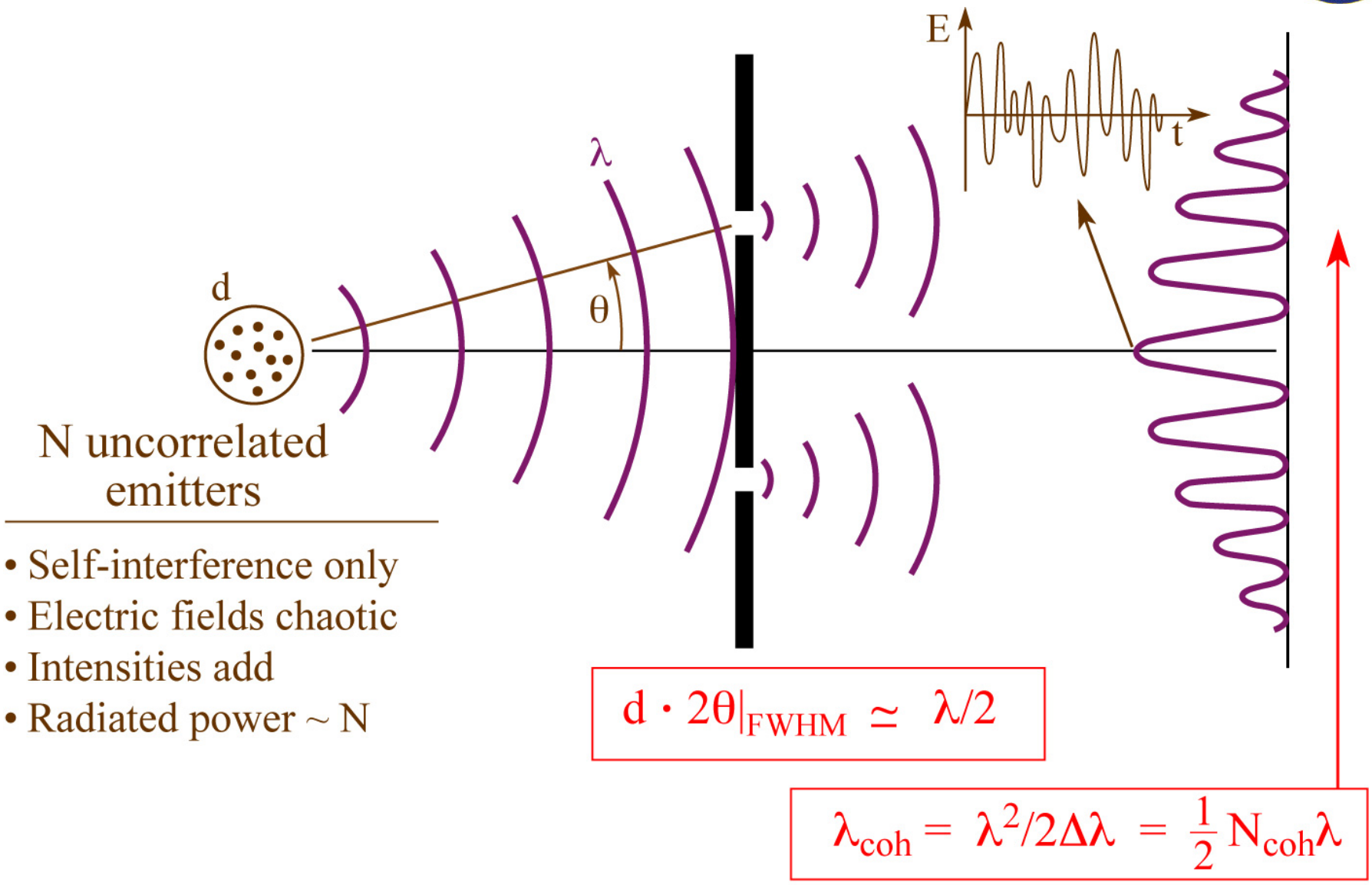

YoungsExprmt_Random_Sept2011.ai

Young's double slit experiment with phase coherent emitters (some lasers, or properly seeded FELs)

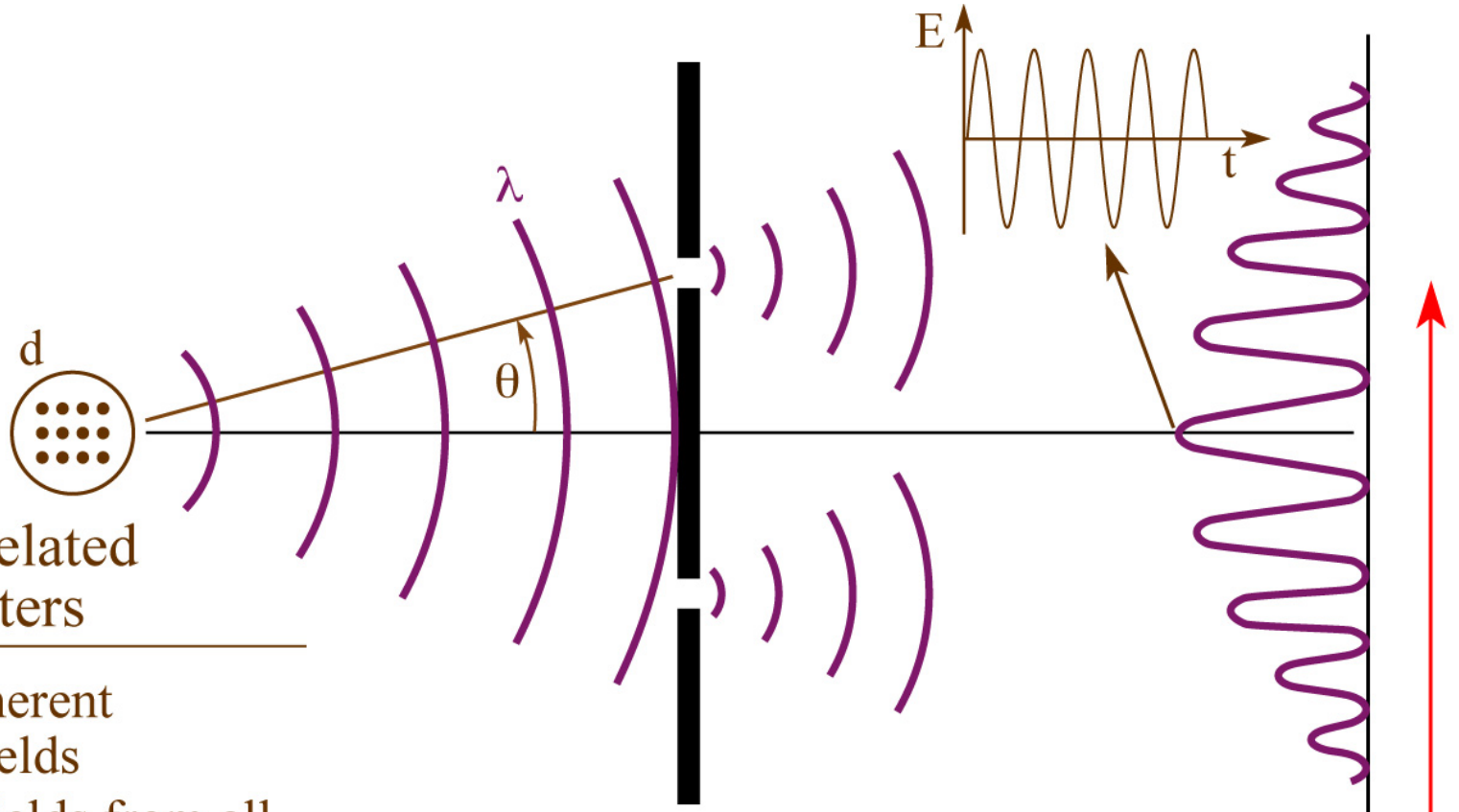

- Phase coherent electric fields
- Electric fields from all particles interfere constructively
- Radiated power ~ N^2
- New phase sensitive probing of matter possible

$$d \cdot 2\theta|_{FWHM} \simeq \lambda/2$$

$$\lambda_{coh} = \lambda^2/2\Delta\lambda = \frac{1}{2} N_{coh}\lambda$$

YoungsExprmt_PhaseCoh_Sept2011.ai

Undulators and FELs

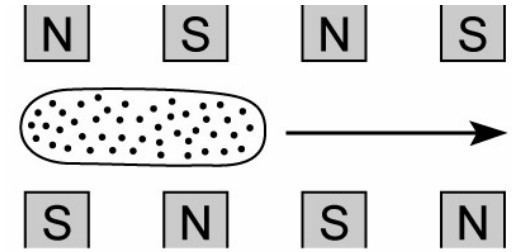

$$\frac{d\mathbf{p}}{dt} = -e(\mathbf{E} + \mathbf{v} \times \mathbf{B})$$

Undulator – uncorrelated electron positions, radiated fields uncorrelated, intensities add, limited coherence, power ~ N.

UndulatorsAndFELs1.ai

Undulators and FELs

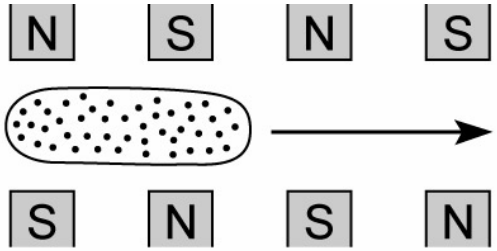

$$\frac{d\mathbf{p}}{dt} = -e(\mathbf{E} + \mathbf{v} \times \mathbf{B})$$

Undulator – uncorrelated electron positions, radiated fields uncorrelated, intensities add, limited coherence, power ~ N.

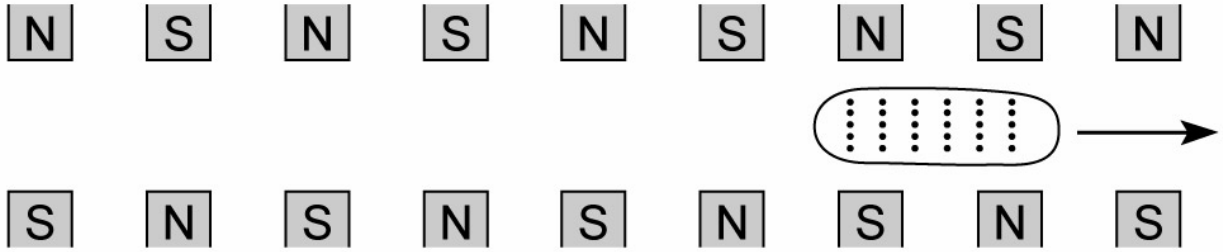

Free Electron Laser (FEL) – very long undulator, electrons are "microbunched" by their own radiated fields into strongly correlated waves of electrons, all radiated electric fields now add, spatially coherent, power ~ N^2

$$\frac{d\mathbf{p}}{dt} = -e(\mathbf{E} + \mathbf{v} \times \mathbf{B})$$

Undulators and FELs

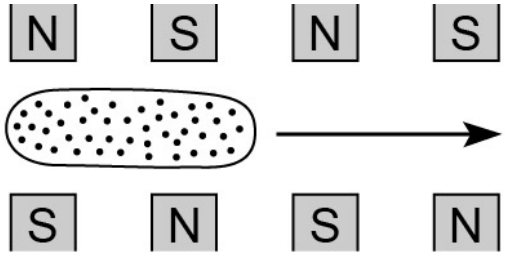

$$\frac{d\mathbf{p}}{dt} = -e(\mathbf{E} + \mathbf{v} \times \mathbf{B})$$

SASE spectrum

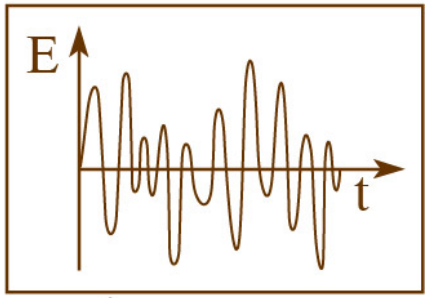

Undulator – uncorrelated electron positions, radiated fields uncorrelated, intensities add, limited coherence, power ~ N.

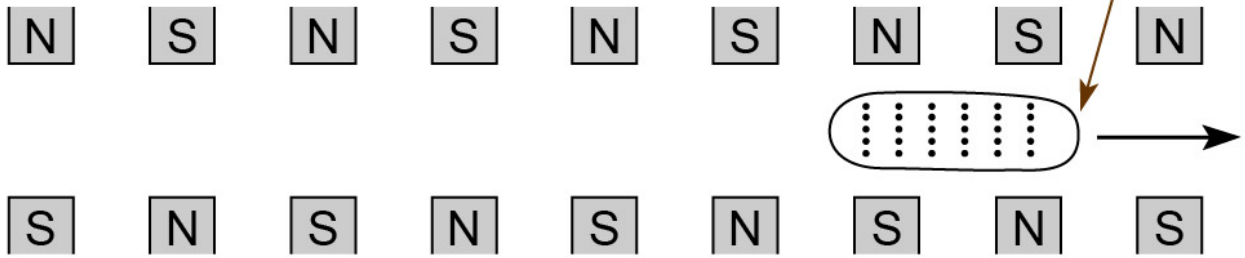

Free Electron Laser (FEL) – very long undulator, electrons are "microbunched" by their own radiated fields into strongly correlated waves of electrons, all radiated electric fields now add, spatially coherent, power ~ N^2

$$\frac{d\mathbf{p}}{dt} = -e(\mathbf{E} + \mathbf{v} \times \mathbf{B})$$

UndulatorsAndFELs2_Sept2013.ai

Seeded FEL

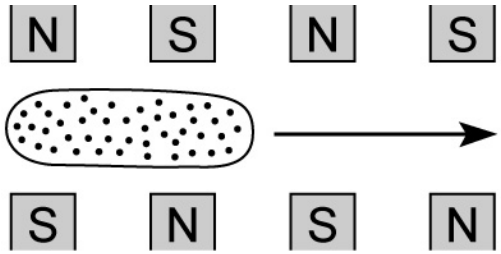

$$\frac{d\mathbf{p}}{dt} = -e(\mathbf{E} + \mathbf{v} \times \mathbf{B})$$

Undulator – uncorrelated electron positions, radiated fields uncorrelated, intensities add, limited coherence, power ~ N.

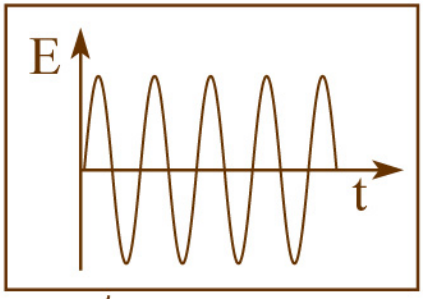

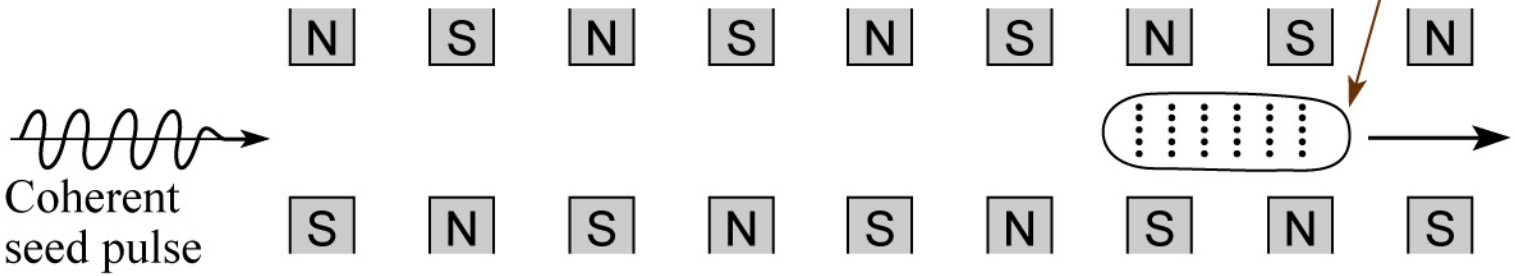

Free Electron Laser (FEL) – very long undulator, electrons are "microbunched" by their own radiated fields into strongly correlated waves of electrons, all radiated electric fields now add, spatially coherent, power ~ N^2

$$\frac{d\mathbf{p}}{dt} = -e(\mathbf{E} + \mathbf{v} \times \mathbf{B})$$

Second generation x-ray FELs.

FEL Microbunching

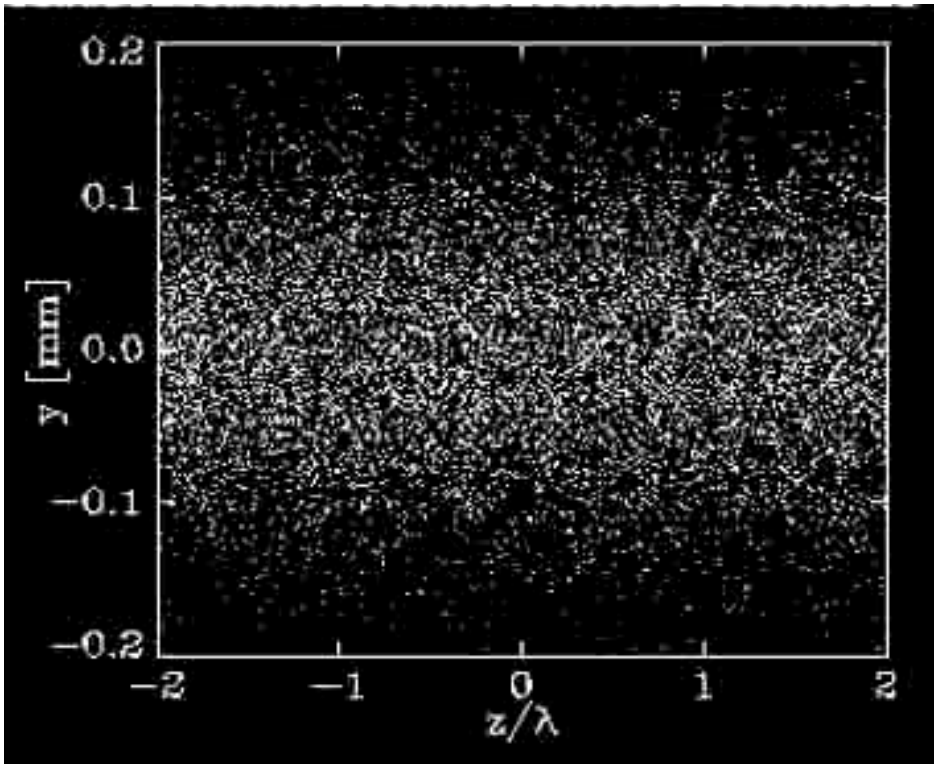

Courtesy of Sven Reiche, UCLA, now SLS

Gain and saturation in an FEL

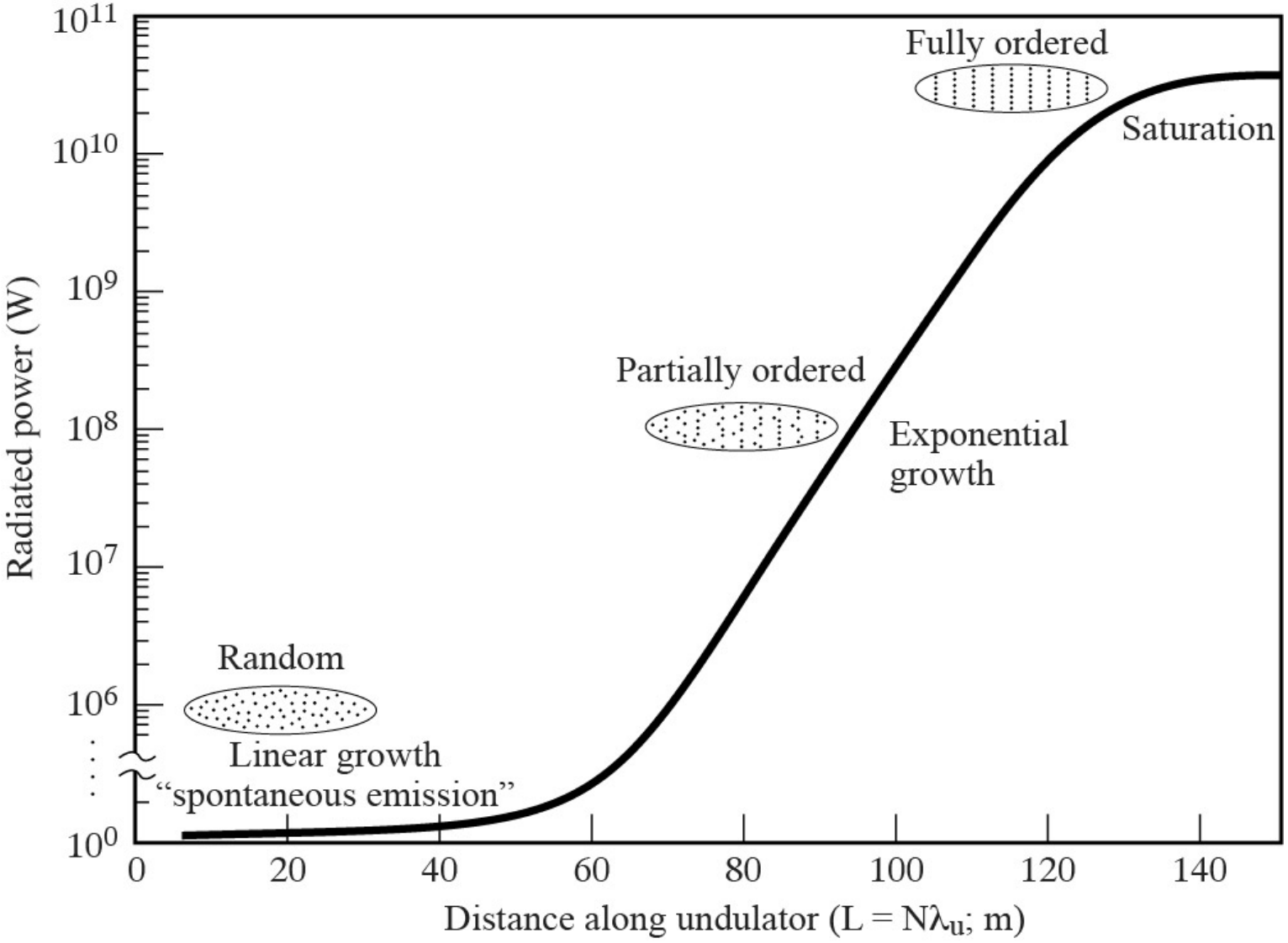

Free electron lasers

Parameters	Flash FEL (Hamburg 2005)	Fermi (Trieste, 2010)	LCLS (Stanford, 2009)	SACLA (Hyogo, 2011)	EU XFEL (Hamburg, 2015)
E_e	1.25 GeV	1.24 GeV	13.6 GeV	8 GeV	17.5 GeV
γ	2,450	2,300	26,600	15,700	35,000
$\hat{I}$	1.3 kA	300 A	3.4 kA	3 kA	5 kA
λ_u	27.3 mm	55 mm	30 mm	18 mm	35.6 mm
N	989	216	3733	4986	4000
L_u	27 m	14 m	112 m	90 m	200 m
$\hbar\omega$	30-300 eV (4-40 nm)	20-60 eV (20-60 nm)	250 eV - 12 keV (1-50 Å)	4.5-15 keV (0.8-2.8 Å)	4-12 keV (1-3 Å)
$\lambda/\Delta\lambda_{FWHM}$	100	1000	200-500	200-400	1000
$\Delta\tau_{FWHM}$	25 fsec	85 fsec	70 fsec	30 fsec	100 fsec
$\dot{\mathcal{F}}$ (ph/pulse)	3×10^{12}	5×10^{12}	2×10^{12}	5×10^{11}	10^{12}
rep rate	5 Hz	10 Hz	120 Hz	60 Hz	5 Hz
$\hat{P}$	1 GW	1 GW	25 GW	30 GW	20 GW
L	260 m	200 m	2 km	710 m	3.4 km
Polarization	linear	variable	linear	linear	variable (?)
Mode	SASE	Seeded (3ω Ti: saphire)	SASE	SASE	SASE

Flash II, Fermi II, SLS FEL, LCLS II, ...

FreeElectronLasersChart_Sept2013.ai

References

1) D. Attwood, *Soft X-Rays and Extreme Ultraviolet Radiation* (Cambridge, UK, 2000); available at Amazon.com.
2) J. Samson and D. Ederer, *Vacuum Ultraviolet Spectroscopy I and II* (Academic Press, San Diego, 1998). Paperback available.
3) J. Als-Nielsen and D. McMorrow, *Elements of Modern X-ray Physics* (Wiley, New York, 2001), 2nd edition (paperback).
4) A. Hofmann, *Synchrotron Radiation* (Cambridge, UK, 2004).
5) P. Duke, *Synchrotron Radiation* (Oxford, UK, 2000)
6) P. Schmüser, M. Dohlus, J. Rossbach, *Ultraviolet and Soft X-Ray Free-Electron Lasers* (Springer-Verlag, Berlin, 2008)

Ch05_ReferencesSept2012.ai

Lectures online at www.youtube.com

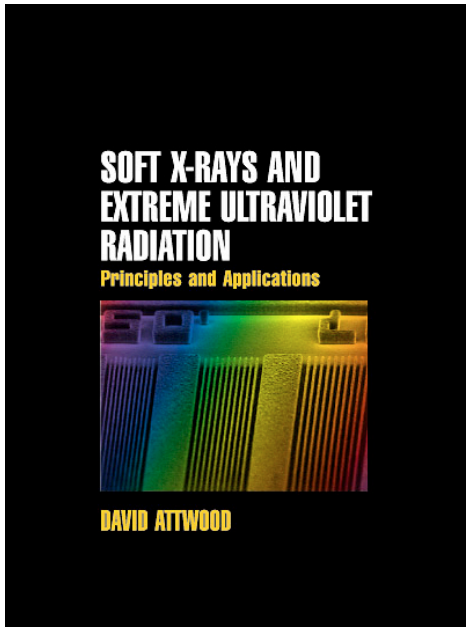

Amazon.com

UC Berkeley

www.coe.berkeley.edu/AST/sxreuv

www.coe.berkeley.edu/AST/srms

www.coe.berkeley.edu/AST/sxr2009